Marine and Petroleum Geology 67 (2015) 635–652

Contents lists available at ScienceDirect

Marine and Petroleum Geology

journal homepage: www.elsevier.com/locate/marpetgeo

Research paper

Source rock characteristics and hydrocarbon expulsion potential of the Middle Eocene Wenchang formation in the Huizhou depression, Pearl River Mouth basin, south China sea

Hang Jiang [a, b], Xiongqi Pang [a, b, *], Hesheng Shi [c], Qiuhua Yu [c], Zhe Cao [a, b], Rui Yu [a, b], Di Chen [a, b], Zulie Long [c], Fujie Jiang [a, b]

[a] State Key Laboratory of Petroleum Resources and Prospecting, China University of Petroleum, Beijing 102249, China
[b] College of Geosciences, China University of Petroleum, Beijing 102249, China
[c] China National Offshore Oil Corporation Limited-Shenzhen, Guangzhou 510240, China

ARTICLE INFO

Article history:
Received 12 March 2015
Received in revised form
25 May 2015
Accepted 15 June 2015
Available online 18 June 2015

Keywords:
Source rock
Geochemical characteristics
Hydrocarbon expulsion
Huizhou depression
Pearl River Mouth basin
South China sea

ABSTRACT

The Middle Eocene Wenchang (WC) formation in the Huizhou depression of the Pearl River Mouth basin is an important geological element for petroleum exploration in the South China Sea. In this study, the geological and geochemical characteristics of the WC source rocks, including the distribution, sedimentary environment, organic matter type, hydrocarbon generation potential and thermal maturity were investigated. Hydrocarbon generation history and hydrocarbon expulsion intensity and quantities were evaluated through one dimensional basin modelling and an improved hydrocarbon generation potential methodology. The WC source rocks are widely distributed and have an elevated thickness (mostly thicker than 200 m, with a maximum thickness greater than 1000 m); they were deposited in a lacustrine weak oxidation–weak reduction sedimentary environment with low salinity. The source rocks have low to high organic matter abundance (TOC mainly ranges from 0.27 to 3.59 wt% with an average of 1.39 wt%) dominated by II_1–type and II_2–type kerogen, resulting in significant hydrocarbon generating potential under moderate–high thermal evolution (R_o mainly ranges from 0.65% to 1.2% on the margins of sags and greater than 1.2% in the centre of sags). The source rocks became mature (R_o = 0.5%) in the early Miocene and began to generate hydrocarbons. They reached the hydrocarbon expulsion threshold at 0.8% R_o and the hydrocarbon expulsion rate became greatest at 1.1% R_o. The expulsion intensities in the H26 sag, H21 sag, X24 sag and X23 sag are relatively large, with their greatest expulsion intensities being 104×10^6, 71×10^6, 62×10^6 and 53×10^6 t/km^2, respectively. The comprehensive hydrocarbon expulsion efficiency was approximately 75%. About 690.1×10^8 t of hydrocarbons were expulsed from the WC source rocks in the Huizhou depression.

1. Introduction

The Pearl River Mouth basin (PRMB) is one of the most petroliferous basins in China (Chen, 2000; Guo et al., 2000). The Huizhou depression, located in the northern part of the Pearl River Mouth basin, has enormous inferred hydrocarbon resources. Many oil fields have been recently discovered in the Huizhou depression. The oil and natural gas resources are huge, with approximately 3.88 billion tons and 0.27 billion tons, respectively (Shi et al., 2009), making it an important and strategic area for petroleum exploration (Fu et al., 2001; Wu et al., 2012). At present, 32 oil fields have been identified in the Huizhou depression and its surrounding areas. The hydrocarbons in these oil fields are discovered in the Late Oligocene Zhuhai formation and the early to middle Miocene Zhujiang formation and Hanjing formation (Zhang et al., 2003, 2004). The sources of these hydrocarbons are mainly from Eocene Wenchang formation and secondary from early Oligocene Enping

* Corresponding author. State Key Laboratory of Petroleum Resources and Prospecting, China University of Petroleum, 18 Fuxue Road, Changping District, Beijing, 102249, China.
E-mail addresses: victoriajh86@aliyun.com (H. Jiang), pangxq@cup.edu.cn (X. Pang).

http://dx.doi.org/10.1016/j.marpetgeo.2015.06.010
0264-8172/

formation (Zhang et al., 2003, 2004; Li et al., 2008). The total reserves are estimated by the China National Offshore Oil Corporation Limited-Shenzhen in the order of millions of cubic meters. This demonstrates that the Huizhou depression is one of the major hydrocarbon–rich areas in the PRMB (Chen, 2000; Guo, 2000; Shi et al., 2009). Despite the huge inferred resource potential, successfully locating the accumulations has been challenging, and currently only 15% of the potential resource been discovered (Wu et al., 2012).

With the continuous increase of petroleum exploration in the Neogene formations, there has been an extensive prospecting in the shallower Miocene and Oligocene age succession. It has become increasingly difficult to prospect for large oil and gas fields in these strata. Therefore, the exploration target has gradually been shifted to the deeper Eocene strata (Zhu et al., 1997; Wang and Zhang, 1999; Zhu et al., 1999; Nie et al., 2001; Shi, 2013). Large amounts of data indicate that the Middle Eocene mudstone–bearing Wenchang (WC) formation in the Huizhou depression contains the main source rocks (Yuan et al., 2014). Poor knowledge of the characteristics and evolution of the organic matter within the potential source rocks may have been responsible for the unsuccessful exploration attempts in the Huizhou depression. Therefore, knowledge of whether the Middle Eocene source rocks have generated and expelled a high petroleum volume is critical.

This study focuses on the detailed geochemistry of the Middle Eocene WC formation in the Huizhou depression to provide an overview of the source rock characteristics. This work analyses the distribution, sedimentary environment, hydrocarbon generation potential and thermal maturity of the organic matter. Moreover, it systematically evaluates the hydrocarbon generation history and hydrocarbon expulsion characteristics, including expulsion intensity, efficiency and expelled hydrocarbon quantities. The final purpose of this work is to re–appraise and validate the potential of the WC formation as an effective source rock to ultimately provide further insight into the source rocks for future petroleum exploration programs and resource assessments in the basin.

2. Geological setting

The Pearl River Mouth basin (PRMB), located in the South China Sea (Fig. 1a), is divided into five tectonic units from north to south (Fig. 1b). These are the northern uplift zone, the northern depression zone, the central uplift zone, the southern depression zone and the southern uplift zone. The Huizhou depression is located in the central part of the Zhu I subbasin, which is part of the northern depression zone (Fig. 1c). The Huizhou depression stretches from the northern uplift in the north to the central uplift in the south, and from the H–L low uplift in the east to the H-X uplift in the west, with an area of approximately 10,000 km^2. The PRMB, which formed as a result of complex poly-extensional tectonic evolution, can be subdivided into three main tectonic stages: (1) Late Cretaceous to early Oligocene rifting stage. (2) Middle Oligocene to early–middle Miocene depression stage. (3) Late Miocene to the present block–faulting stage (Robinson et al., 1998; Zhang et al., 2004; Cui et al., 2009). During this period, tectonic movements resulted in a series of uplifted and subsided blocks (Zhang et al., 2004; Cui et al., 2009).

The geological setting controls the structural configuration of the Huizhou depression, consequently influences the source rock characteristics and hydrocarbon generation and expulsion history. The Huizhou depression experienced continental mudstone deposition within fluvial and lacustrine environments during most of the Paleogene and Eocene rifting episode (Aquilera et al., 1990; Chen and Pei, 1993; Robison et al., 1998; Zhu et al., 2009; Sun et al., 2012), developing 11 sags during this rifting episode (Fig. 1c) (Xu et al., 2012). In the Middle Eocene, the shallow to semi-deep lacustrine organic–rich mudstones were deposited in the 11 sags, forming the primarily important Wenchang (WC) source rocks (Zhang et al., 2003; Xu et al., 2012). The maximum thickness is approximately 2500 m (Xu et al., 2012). In the Late Eocene, a suit of fluvial swamp facies coal-bearing strata were deposited, forming the secondarily important Enping (EP) source rocks (Xu et al., 2012; Li et al., 2013; Wu et al., 2013), with the mudstone and coal-bearing beds of different thickness. The thickness of EP formation in the centre of sag was not greater than 2000 m (Xu et al., 2012).

Subsequently, the Huizhou depression subsided slowly and most of the depression was occupied by shallow seawater during the middle Oligocene (Zhang et al., 2004; Cui et al., 2009). Sandstone beds with high porosity and permeability, in combination with marine shale, formed excellent reservoir–seal assemblages (Fig. 2) (Zhu et al., 1999; Gong and Li, 2004; Zhou, 2011; Cheng et al., 2013).

3. Materials and methods

3.1. Materials

72 core samples from five wells in the Huizhou depression were collected for source rock analysis. Information on core samples is provided in Table 1 along with sample well location (Fig. 1). All the wells are generally concentrated on a structural high within the depression. Three wells (HZ1, HZ2 and HZ4) were drilled to the bottom of the WC formation, and the other two wells were drilled below the top of the WC formation in the study area. All samples were obtained from mudstones sections. The lithologies of the samples comprise a variety of organic-rich mudstones, silty mudstone and carbonaceous mudstone. Furthermore, TOC distribution map of the WC formation was selected from Shi (2013). Formation thicknesses and lithologies data of well HZ1, HZ2 and HZ4, which were drilled to the bottom of the WC formation, were collected from well drilling reports for the 1D basin modelling (Table 2). Geothermal gradient data were also collected from well drilling reports. Geothermal gradient of HZ1, HZ2, and HZ4 are 3.23 °C/100 m, 3.22 °C/100 m, and 3.63 °C/100 m, respectively.

3.2. Laboratory methods

3.2.1. Geochemical analyses

The geochemical analyses used to evaluate source rock potential included the determination of total organic carbon (TOC) content, Rock–Eval pyrolysis, and vitrinite reflectance (Ro). The TOC was determined using a LECO CS–400 analyser. Rock–Eval pyrolysis (Espitalié et al., 1977; Peters, 1986) was performed using a Rock–Eval II instrument. The parameters measured included free and volatile hydrocarbon (S_1), which is thermally liberated from a sample at 300 °C, remaining hydrocarbon generative potential (S_2), which arises during progressive heating from 300 to 600 °C (Espitalié et al., 1977; Tissot and Welte, 1984), and temperature of maximum pyrolysis yield (T_{max}). Vitrinite reflectance measurements were conducted on 22 samples with varying TOC contents between 0.37 wt % and 2.89 wt % (Table 3). Measurements of mean random vitrinite reflectance (R_o) were made using an oil immersion lens and a Leica MPV Compact II reflected light microscope fitted with a microphotometer. One hundred point–count measurements were made per sample. The reflectance for each sample was calculated by averaging the histogram of the reliable data (Waples, 1985; Lee, 1997). Furthermore, the hydrogen index (HI) and production index (PI) were calculated using the pyrolysis data (Table 1).

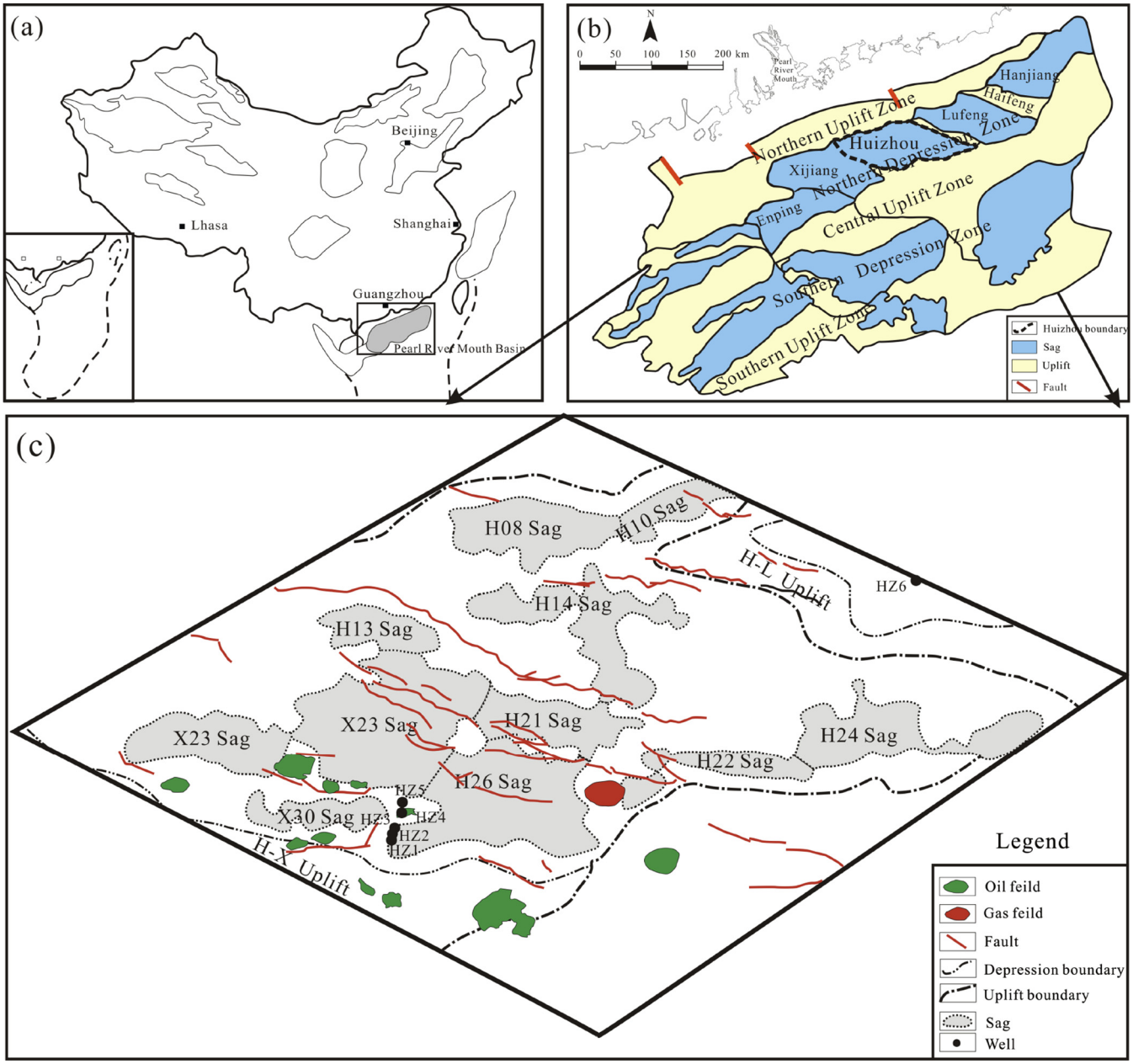

Fig. 1. Map showing the distribution of tectonic units and profile structural characteristics of the Huizhou depression, PRMB and the location of the Huizhou depression, Pearl River Mouth Basin.

Extractable organic matter was obtained by traditional Soxhlet extraction using chloroform, and further analysed through gas chromatography–mass spectrometry (GC–MS) to examine the biomarker geochemistry. The oven temperature was programmed to go from 80 to 290 °C at 4 °C/min, followed by an isothermal period of 15 min. Helium was used as the carrier gas. Compounds were identified by combined gas chromatography/mass spectrometry (GC/MS) using an Agilent GC6890 Plus/MS5973 network system quadrupole instrument using the electron ionization mode (electron energy 70 eV, ion source temperature 230 °C, scanning from 20 to 750 Da at 3 scans/s).

3.2.2. Burial history and thermal maturity modelling

Schlumberger's PetroMod (1D) modelling software (version 10) was used for the reconstruction of the burial and thermal maturity histories of the studied wells. Subsidence curves were constructed for the three wells using formation thicknesses and lithologies assigned from composite well logs (Table 2). The thermal history of sedimentary basins can be evaluated based on the burial history and on the heat-flow evolution (Allen and Allen, 1990; Hakimi and Abdullah, 2015). The heat flow values derived from present-day geotherms suggest heat flow may currently be 65 mW/m^2 in the northern depression zone (Shi et al., 2003).

3.2.3. Hydrocarbon expulsion modelling

The method used in this study was the hydrocarbon generation potential model proposed by Pang et al. (2005) (Fig. 3). We used this model and improved its restoration of the original hydrocarbon generation potential based on mass balance to calculate the expelled hydrocarbon quantities.

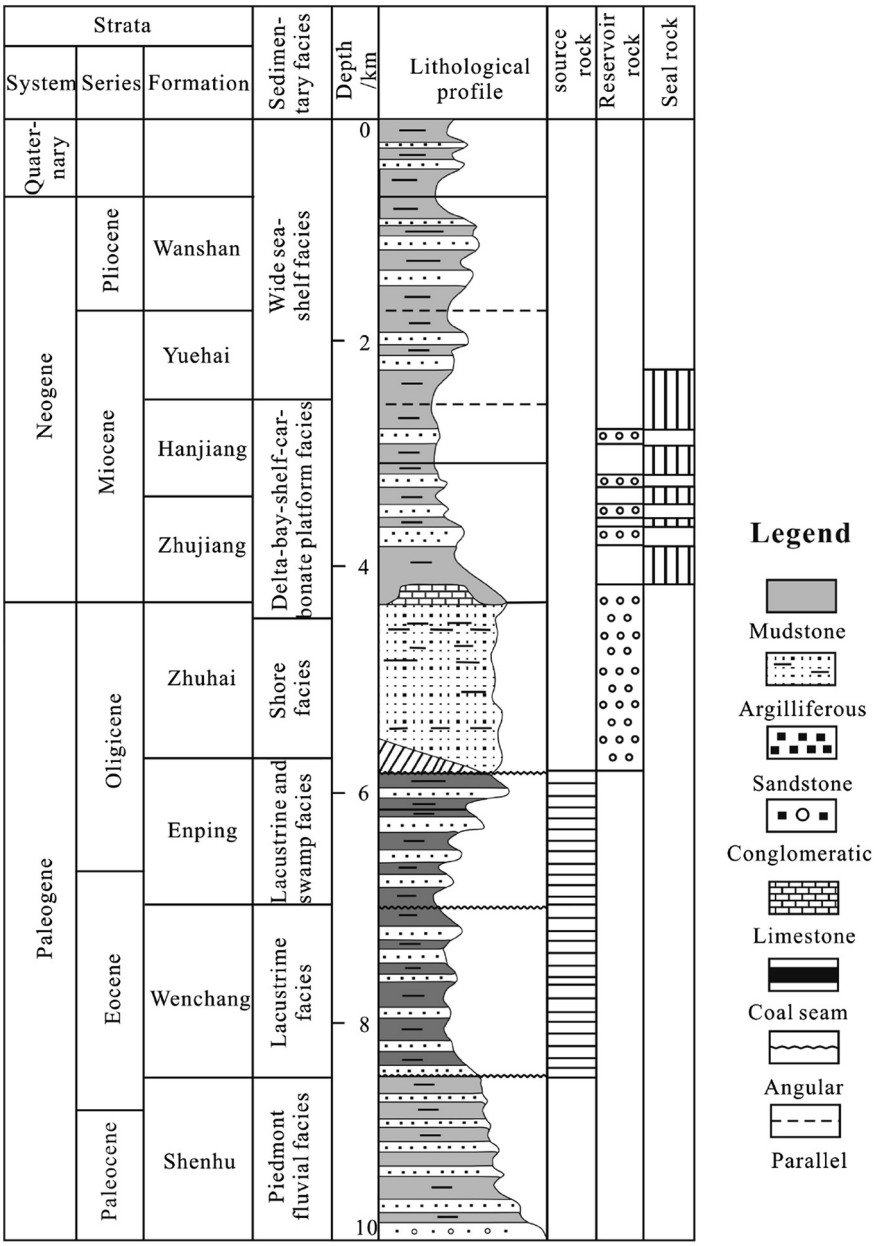

Fig. 2. Stratigraphic column and source-reservoir-seal assemblage of the Huizhou depression (modified after Xu et al., 2012).

The (S_1+S_2)/TOC ratio can be used to reflect the total potential of expelled hydrocarbons, and is called the hydrocarbon generation potential index (GPI) (Zhou and Pang, 2002). Hydrocarbon expulsion occurs when the hydrocarbon generation potential decreases (Fig. 3; Pang et al., 2005; Guo et al., 2014), and the corresponding geological condition is defined as the hydrocarbon expulsion threshold (Zhou and Pang, 2002; Pang et al., 2005). Before hydrocarbons begin to be expelled, the hydrocarbon generation potential index is called the original hydrocarbon generation potential index (GPI_o) (Fig. 3). Here, the original hydrocarbon generation potential index (GPI_o) represents both the hydrocarbon generation potential of the source rock and the retained hydrocarbons.

When hydrocarbon expulsion occurs, the hydrocarbon generation potential index decreases. The residual (S_1+S_2)/TOC ratio is defined as the residual hydrocarbon generation potential index (GPI_r) (Fig. 3).

Zhong et al. (2004) and Zhou (2009) suggested that the consumption amount of organic matter during hydrocarbon expulsion does not completely equal the decrease in the TOC. Thus, the residual hydrocarbon generation potential (GPI_r) measured in samples below the hydrocarbon generation threshold is greater than the real residual hydrocarbon generation potential (GPI_{ro}). The TOC changes under the influence of both organic matter and inorganic matter. Therefore, it is necessary to accurately restore the TOC value to that in the original state at the beginning of hydrocarbon expulsion using the following equations based on the mass balance principle.

$$k = TOC_{ro}/TOC_r \tag{1}$$

$$GPI_{ro} = (S_1 + S_2) \times 100/TOC_{ro} \tag{2}$$

Table 1
Bulk geochemical results of Rock-Eval/TOC analysis and calculated parameters of samples from the WC Formation in the studied wells.

Sample no.	Well no.	Formation	Depth (m)	TOC (%)	T_{max} (°C)	S_1 (mg HC/g rock)	S_2 (mg HC/g rock)	PI	HI (mg HC/g TOC)
1	HZ1	WC	3556.5	0.30	441	0.15	0.54	0.22	180.00
2	HZ1	WC	3562.5	0.27	435	0.1	0.36	0.22	133.33
3	HZ1	WC	3574.5	0.40	436	0.16	0.49	0.25	122.50
4	HZ1	WC	3577.5	0.39	445	0.2	0.72	0.22	184.62
5	HZ1	WC	3582	0.45	443	0.13	0.57	0.19	126.67
6	HZ1	WC	3589.5	0.36	436	0.16	0.58	0.22	161.11
7	HZ1	WC	3595.5	0.35	441	0.11	0.42	0.21	120.00
8	HZ1	WC	3688.5	0.41	438	0.34	0.72	0.32	175.61
9	HZ1	WC	3712.5	0.99	455	0.38	1.1	0.26	111.11
10	HZ1	WC	3745.5	0.44	444	0.17	0.5	0.25	113.64
11	HZ1	WC	3768	2.26	443	1.81	5.14	0.26	227.43
12	HZ1	WC	3805.5	2.59	451	2.21	6.03	0.27	232.82
13	HZ1	WC	3844.5	1.02	449	0.65	1.28	0.34	125.49
14	HZ1	WC	3847	0.76	452	0.18	1.14	0.14	150.00
15	HZ1	WC	3850	2.95	453	2.41	5.9	0.29	200.00
16	HZ1	WC	3859.5	2.16	444	1.06	4.05	0.21	187.50
17	HZ1	WC	3862.5	1.92	450	0.77	3.8	0.17	197.92
18	HZ1	WC	3880.5	3.59	453	2.44	7.42	0.25	206.69
19	HZ1	WC	3883.5	1.98	449	0.77	3.37	0.19	170.20
20	HZ1	WC	3888	2.38	448	1.71	4.38	0.28	184.03
21	HZ1	WC	3892.5	2.64	450	1.3	4.27	0.23	161.74
22	HZ1	WC	3898.5	2.22	450	1.77	4.65	0.28	209.46
23	HZ2	WC	3760.12	0.76	470	0.23	1.02	0.18	134.21
24	HZ2	WC	3768.12	0.46	444	0.13	0.92	0.12	200.00
25	HZ2	WC	3770.12	0.37	419	0.12	0.57	0.17	154.05
26	HZ2	WC	3771.12	0.39	422	0.12	0.64	0.16	164.10
27	HZ2	WC	3774.12	0.55	440	0.14	0.96	0.13	174.55
28	HZ4	WC	3715.5	0.86	450	0.12	0.39	0.24	45.35
29	HZ4	WC	3718.5	0.80	443	0.11	0.78	0.12	97.50
30	HZ4	WC	3721.5	1.70	445	0.20	1.53	0.12	90.00
31	HZ4	WC	3727.5	1.22	448	0.23	1.18	0.16	96.72
32	HZ4	WC	3733.5	1.46	448	0.35	2.18	0.14	149.32
33	HZ4	WC	3733.5	1.72	449	0.54	3.15	0.15	183.14
34	HZ4	WC	3736.5	1.86	451	0.51	2.41	0.17	129.57
35	HZ4	WC	3748.5	1.71	450	0.61	3.44	0.15	201.17
36	HZ4	WC	3754.5	0.99	453	0.28	1.11	0.20	112.12
37	HZ4	WC	3757.5	1.51	449	0.37	2.86	0.11	189.40
38	HZ4	WC	3763.5	2.17	452	0.46	5.02	0.08	231.34
39	HZ4	WC	3766.5	2.89	448	0.69	9.73	0.07	336.68
40	HZ4	WC	3769.5	2.84	462	0.27	6.47	0.04	227.82
41	HZ4	WC	3772.5	3.03	447	0.69	9.20	0.07	303.63
42	HZ4	WC	3772.5	2.69	453	0.45	6.35	0.07	236.06
43	HZ4	WC	3781.5	1.07	448	0.20	1.86	0.10	173.83
44	HZ4	WC	3784.5	1.25	457	0.44	2.01	0.18	160.80
45	HZ4	WC	3787.5	0.52	446	0.47	0.81	0.37	155.77
46	HZ4	WC	3790.5	1.36	449	0.29	2.70	0.10	198.53
47	HZ4	WC	3802.5	1.25	445	0.12	1.28	0.09	102.40
48	HZ4	WC	3826	1.08	447	0.12	1.31	0.08	121.30
49	HZ4	WC	3838.5	1.28	447	0.18	2.81	0.06	219.53
50	HZ4	WC	3856	1.01	445	0.09	1.33	0.06	131.68
51	HZ4	WC	3856.5	1.28	448	0.13	1.79	0.07	139.84
52	HZ4	WC	3874.5	1.47	445	0.18	2.46	0.07	167.35
53	HZ4	WC	3891.5	0.96	446	0.08	1.34	0.06	139.58
54	HZ4	WC	3895.5	0.74	443	0.10	1.23	0.08	166.22
55	HZ4	WC	3907.5	1.13	448	0.12	1.68	0.07	148.67
56	HZ4	WC	3919.5	1.00	446	0.11	1.55	0.07	155.00
57	HZ4	WC	3931.5	0.77	446	0.06	0.93	0.06	120.78
58	HZ4	WC	3946.5	0.70	446	0.07	1.09	0.06	155.71
59	HZ5	WC	3976.0	1.23	438	0.36	2.98	0.11	242.28
60	HZ5	WC	4066.5	0.67	442	0.28	2.11	0.12	314.93
61	HZ5	WC	4096.5	0.89	445	0.38	2.21	0.15	248.31
62	HZ5	WC	4096.5	2.14	455	0.52	2.73	0.16	127.57
63	HZ5	WC	4102.5	1.97	448	0.71	3.71	0.16	188.32
64	HZ5	WC	4132.5	3.24	454	0.47	4.06	0.10	125.31
65	HZ5	WC	4165.5	0.83	464	0.23	0.84	0.21	101.20
66	HZ5	WC	4180.5	2.43	444	0.99	6.41	0.13	263.79
67	HZ5	WC	4195.5	1.96	446	1.04	3.80	0.21	193.88
68	HZ5	WC	4204.5	1.20	473	0.27	1.52	0.15	126.67
69	HZ5	WC	4224.5	1.64	454	0.61	2.03	0.23	123.78
70	HZ6	WC	3312.5	1.32	442	0.19	1.9	0.09	143.94
71	HZ6	WC	3742.5	1.14	442	0.12	1.47	0.08	128.95
72	HZ6	WC	3972.0	1.42	443	0.16	1.99	0.07	140.14

Table 2
Input data for modelling of depositional and erosional events of studied wells (HZ1, HZ2, and HZ4) in the Huizhou depression.

Age	Fm	Lithology	Deposition age		Erosion age		Erosion (m)	Respective wells in the Huizhou depression (see Fig. 1)								
								HZ1 well			HZ2 well			HZ4 well		
			From (Ma)	To (Ma)	From (Ma)	To (Ma)		Top (m)	Bottom (m)	Thickness (m)	Top (m)	Bottom (m)	Thickness (m)	Top (m)	Bottom (m)	Thickness (m)
Paleocene	WS	Sandstone and mudstone	5.5	1.8				204.5	672.5	468	200	663	463	180	507	327
Miocene	YH	Sandstone and mudstone	10	5.5				672.5	948.6	276.1	663	944	281	507	1001.8	494.8
	HJ	Sandstone and mudstone	16.4	10				948.6	1841.7	893.1	944	1856.3	912.3	1001.8	1889.1	887.3
	ZJ	Sandstone and mudstone	23.8	16.4				1841.7	2931.6	1089.9	1856.3	2948.3	1092	1889.1	2975.7	1086.6
Oligocene	ZH	Sandstone	33.9	23.8				2931.6	3347	415.4	2948.3	3386	437.7	2975.7	3367.9	392.2
Eocene	EP	Mudstone	39	35.6	35.6	33.9	75	3347	3576.4	229.4	3386	3538.5	152.5	3367.9	3675.5	307.6
	WC	Mudstone	49	41.4	41.4	39	370	3576.4	3918	341.6	3538.5	4040	501.5	3675.5	3859.2	183.7

Table 3
Random vitrinite reflectance (Ro%) for 22 WC samples in Huizhou depression.

Sample no.	Well no.	depth(m)	TOC(wt%)	Ro(%)
5	HZ1	3582.0	0.45	0.730
8	HZ1	3688.5	0.41	0.714
10	HZ1	3745.5	0.44	0.720
14	HZ1	3847.0	0.76	0.725
16	HZ1	3859.5	2.16	0.740
17	HZ1	3862.5	1.92	0.760
19	HZ1	3883.5	1.98	0.730
20	HZ1	3888.0	2.38	0.730
21	HZ1	3892.5	2.64	0.770
22	HZ1	3898.5	2.22	0.760
23	HZ2	3760.1	0.76	0.700
25	HZ2	3770.1	0.37	0.710
27	HZ2	3774.1	0.55	0.720
29	HZ4	3718.5	0.8	0.681
37	HZ4	3757.5	1.51	0.739
39	HZ4	3766.5	2.89	0.751
44	HZ4	3781.5	1.25	0.723
63	HZ5	4102.5	1.97	0.774
68	HZ5	4204.5	1.20	0.781
70	HZ6	3312.5	1.32	0.656
71	HZ6	3742.5	1.14	0.726
72	HZ6	3972.0	1.42	0.754

$$GPI_r = (S_1 + S_2) \times 100/TOC_r \quad (3)$$

where k is the restoration coefficient; TOC_{ro} is the real residual TOC value of hydrocarbon expulsion (%); TOC_r is the remaining TOC value measured in the samples (%).

Combining Eqs. (1)–(3), we obtain the following Eq. (4):

$$GPI_{ro} = GPI_r/k \quad (4)$$

Therefore, the key to the improved hydrocarbon generation potential method is the proper organic matter abundance (TOC) restoration. The organic matter abundance (TOC) in a source rock is controlled by the qualities of both the source rock and organic matter. According to the mass balance principle, the residual organic carbon quantity is equal to the original organic carbon quantity of the rock minus the sum quantity of the organic carbon taken away by the expelled hydrocarbons and the organic carbon generating carbon dioxide (CO_2). The restoration coefficient can be calculated by the following Eq. (5):

$$k = \frac{1 - 0.83 \times GPI_r/1000}{1 - 0.83 \times GPI_o/1000} \quad (5)$$

where k is the restoration coefficient; 0.83 is the average carbon content in the hydrocarbons (Burnham, 1989; Guo et al., 2014); GPI_r is the remaining hydrocarbon generation potential index (mg HC/g TOC); PGI_o is the hydrocarbon generation potential index at the expulsion threshold (mg HC/g TOC).

The real residual hydrocarbon generation potential GPI_{ro} can be calculated using a combination of Eqs. (4) and (5):

$$GPI_{ro} = \frac{1 - 0.83 \times GPI_o/1000}{1 - 0.83 \times GPI_r/1000} \times GPI_r \quad (6)$$

The hydrocarbon generation potential index at the hydrocarbon

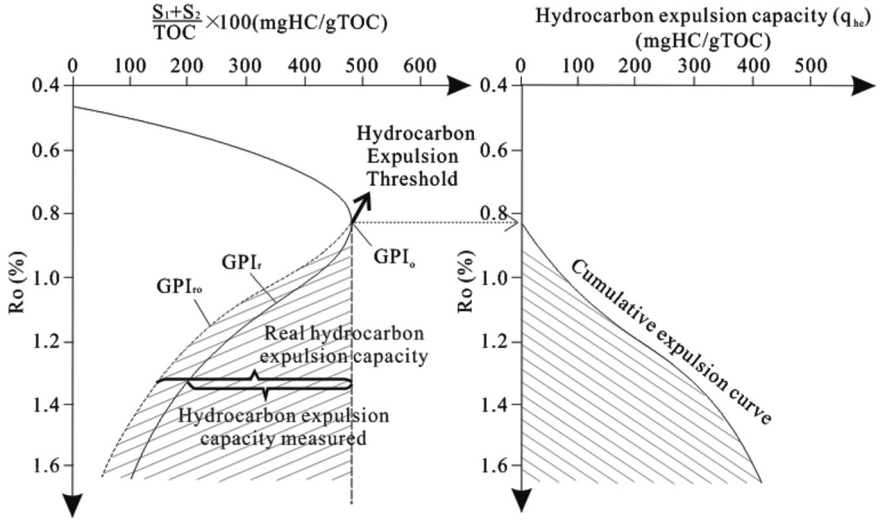

Fig. 3. Operational models for the quantification of hydrocarbon generation and expulsion (modified from Pang et al., 2005).

expulsion threshold is the maximum hydrocarbon generation capacity (q_{hg}) (mg HC/g TOC) of the source rock. The difference between the hydrocarbon generation potential index at the hydrocarbon expulsion threshold and the real residual hydrocarbon generation potential index is the hydrocarbon expulsion capacity (q_{he}) (mg HC/g TOC), which is the hydrocarbon expelled per unit of organic carbon since the source rock passed the hydrocarbon expulsion threshold. The vitrinite reflectance corresponding to the hydrocarbon expulsion threshold is called R_{ot}. When R_o increases after the hydrocarbon expulsion threshold, there is a corresponding increase in the hydrocarbon expulsion rate (r_{he}). The hydrocarbon expulsion rate (r_{he}) at a certain R_o value (R_{oc}) is the derivative of the hydrocarbon expulsion capacity (q_{he}) at R_{oc} (Eq. (7)). The hydrocarbon expulsion intensities (I_{he}) of a certain source rock can be calculated using the following Eq. (8):

$$r_{he}(Ro) = \frac{dq_{he}}{dR_o} \tag{7}$$

$$I_{he} = \int_{R_{ot}}^{R_o} q_{he}(R_o) \times h \times \rho \times TOC(R_o) \times d(R_o) \tag{8}$$

Then, the hydrocarbon expulsion quantities (Q_{he}) can be calculated using the following Eq. (9):

$$Q_{he} = I_{he} \times S = \int_{R_o t}^{R_o} q_{he}(R_o) \times h \times S \times \rho \times TOC(R_o) \times d(R_o) \tag{9}$$

where Q_{he} is the hydrocarbon expulsion quantity at the maturity of R_o (t), $q_{he}(R_o)$ is hydrocarbon expulsion ratio at the maturity of R_o (mg/g), R_o is vitrinite reflectance (%), h is the source rock thickness (m), ρ is source rock density (g/cm^3), TOC is total organic content calculated from TOC isopach maps (%) and S is the source rock area (m^2).

4. Results

4.1. TOC content and rock-eval pyrolysis

TOC content and Rock-Eval pyrolysis results are presented in Table 1. TOC contents vary between 0.27 and 3.59 wt %, and have an average of 1.39 wt %. S_1 values vary between 0.06 and 2.44 mg HC/g rock and have an average of 0.48 mg HC/g rock. S_2 values vary between 0.76 and 9.73 mg HC/g rock and an average of 2.52 mg HC/g rock. HI values vary between 45.4 and 337 mg HC/g TOC and have an average of 167.6 mg HC/g TOC. T_{max} values vary between 419 °C and 473 °C and have an average of 447 °C. PI values vary between 0.04 and 0.37 with an average of 0.16.

4.2. Organic geochemistry

Ratios of different biomarkers were calculated and used for the interpretation of depositional environment and thermal maturity of the studied rock succession. The abundance of short chain n-alkanes ($nC_{14} - nC_{19}$) similar with long chain n-alkanes ($nC_{27} - nC_{31}$) is seen in all analysed samples (Fig. 4). Calculated terrigenous/aquatic ratios, TAR = $(nC_{27} + nC_{29} + nC_{31})/(nC_{15} + nC_{17} + nC_{19})$ (Peters et al., 2005) vary between 0.85 and 1.49 (Table 4). Pristane/phytane (Pr/Ph) ratios range from 1.11 to 2.47 (Table 4). Pr/nC_{17} and Ph/nC_{18} range from 0.448 to 0.784, from 0.207 to 0.566, respectively, and the Pr/nC_{17} and Ph/nC_{18} ratios are plotted in Fig. 5. Identified steranes and hopanes are listed in Table 4. The sterane/hopane ratio of the samples from the Huizhou depression ranges from 0.13 to 0.39 (Table 4). The gammacerane/C30-hopane ratio of the samples ranges from 0.04 to 0.14 (Fig. 4 and Table 4).

5. Discussion

5.1. Geological and geochemical characteristics of source rocks

5.1.1. Source rock distribution

All the wells are located on the margins of sags (Fig. 1c) and thus, the source rock thickness estimations from the wells underestimate the source rock distribution and thickness. In addition to the well data, structural isoline maps of both top and bottom WC formation were incorporated in this study to better describe the source rock distributions and thickness variations (Fig. 6).

Source rocks in the H26 sag, X24 sag, X23 sag, H21 sag and H24 sag are well developed, with the thickness ranging approximately from 400 to 2000 m. The thicknesses in the other sags range approximately from 200 to 800 m (Fig. 7). The source rocks on the H–L uplift are thinner, with thickness ranging approximately from 0 to 600 m. No source rock has been discovered in the northwestern part of this uplift. There are no WC source rocks found in the H–X uplift.

5.1.2. Source rock sedimentary environment

Low Pristane/Phytane values (<1) indicate reducing depositional environments, while values >1 denote the progressive increase of oxygen content, up to ratios >3 that represent terrestrial matter input under pure oxidizing conditions (Peters et al., 1999, 2005; Obermajer et al., 2010; Aali and Rahmani, 2011; Oppo et al., 2013). The intermediate Pr/Ph ratio from 0.8 to 2.5 indicates weak oxidation–weak reduction environments and it cannot be regarded as a definite indicator of the depositional environment (Powell and McKirdy, 1973; Volkman and Maxwell, 1986; Powell, 1988; Amane and Hideki, 1997; Peters et al., 1999; Oppo et al., 2013). The moderate Pr/Ph ratios (1.12–2.02) as well as the Pr/nC17 and Ph/nC18 ratios (Fig. 5) of the WC formation suggest that the WC organic matter was deposited in a weak oxidation–weak reduction environment (Bou Daher et al., 2015).

The low sterane and low sterane/hopane ratio are indicative of terrigenous and/or microbially reworked organic matter (e.g. Tissot and Welte, 1984; Peters and Moldowan, 1993). The sterane/hopane ratio of the samples from the Huizhou depression ranges from 0.13 to 0.39 (Table 3), indicating that the WC formation depositional environment was isolated from marine conditions, and was probably a lacustrine basin. The n-alkane (0.85 < TAR<1.49) shows a dominance of terrestrial organic matter over marine organic matter (Table 3). Gammacerane is a marker for a stratified water column during source rock deposition, commonly associated with elevated salinity (Sinninghe Damsté et al., 1995; Peters et al., 2005). The gammacerane/C30-hopane ratio of the samples ranges from 0.04 to 0.14 (Table 3), indicating that the salinity of the WC formation sedimentary environment was low.

5.1.3. Type of organic matter

The organic matter type can be characterized based on pyrolysis and HI analysis. Generally, Type I and Type II_1 kerogen commonly possess HI values of more than 300 mg HC/g TOC derived from lacustrine and marine source rocks (e.g. Nicholas et al., 2004; Hakimi et al., 2012a,b; Hakimi and Abdullah, 2013), whereas Type II_2 kerogens are comprised of materials with HI values higher than 200 mg HC/g TOC. Source rocks with HI values lower than 200 mg HC/g TOC mainly contain type III kerogens. Based on pyrolysis data, kerogen classification diagrams were constructed to determine the kerogen type and maturity (e.g. Tissot and Welte, 1984;

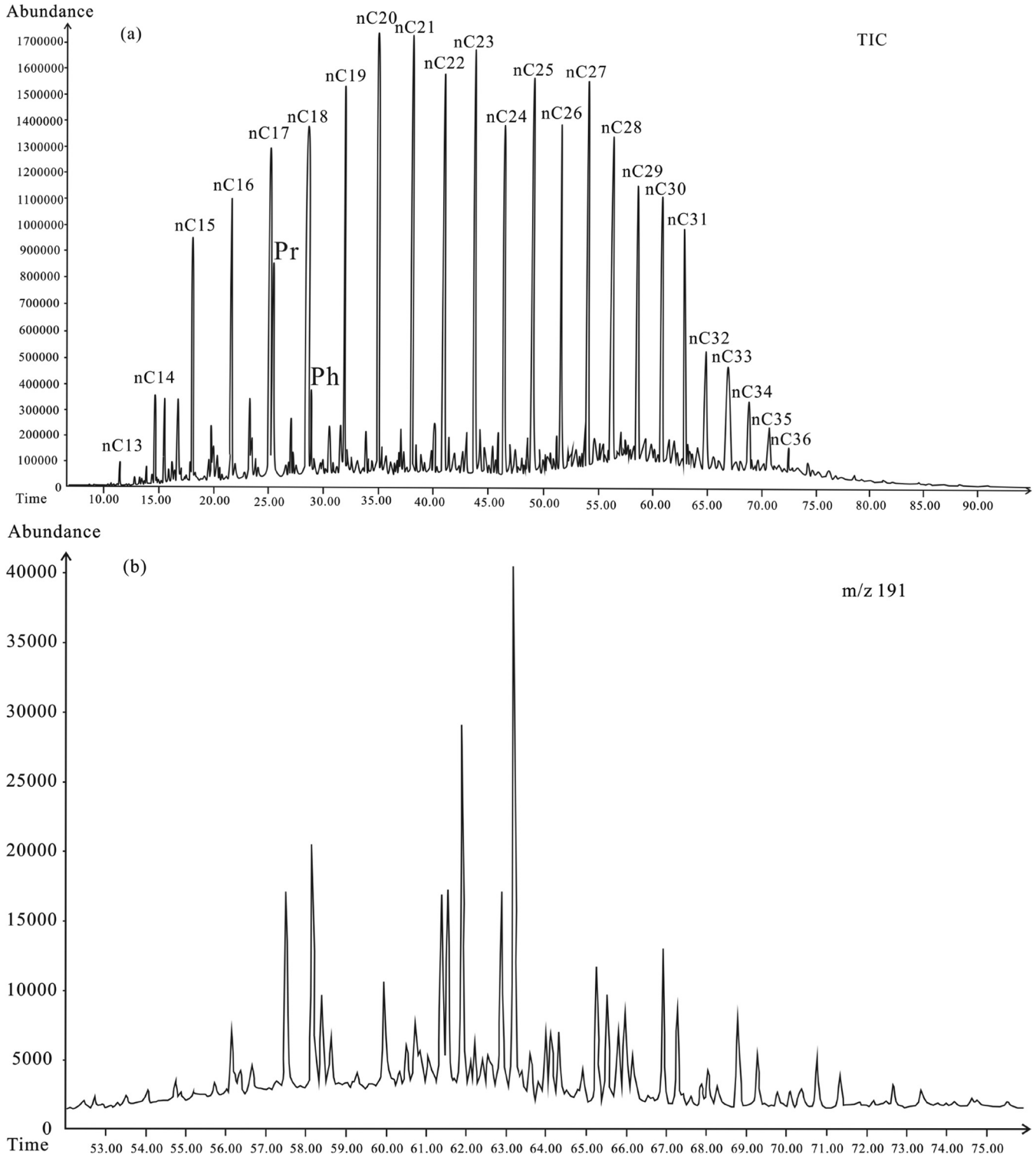

Fig. 4. Gas chromatograms of WC samples. (a, b) HZ4, 3748.5 m, mudstone, samples No. 35, (c,d) HZ5, 3976 m, mudstone, sample No. 59, and (e, f) HZ6,3972.0 m, mudstone, sample No. 72.

Mukhopadhyay et al., 1995). Most of the WC samples plot in the mature zone of Type II_1 and Type II_2 kerogen, with small amounts of Type I and Type III kerogen (Fig. 8a). Samples with burial depth above 3500 m contain Type II_2 kerogen. Samples with burial depth between 3500 m and 4000 m mainly contain Type II_1 and Type II_2 kerogen, while samples with burial depth below 4000 m mainly contain Type II_1 kerogen (Fig. 8b).

5.1.4. Source rock generative potential

The generative potential of the WC formation was evaluated using total organic carbon content (TOC wt%) and pyrolysis S_2 yields (Table 1). Peters (1986) and Peters and Cassa (1994) rated source rocks with a TOC of less than 0.5 as poor source rocks, 0.5–1 as fair source rocks, 1–2 as good source rocks, 2–4 as very good source rocks and more than 4 as excellent source rocks. All the WC

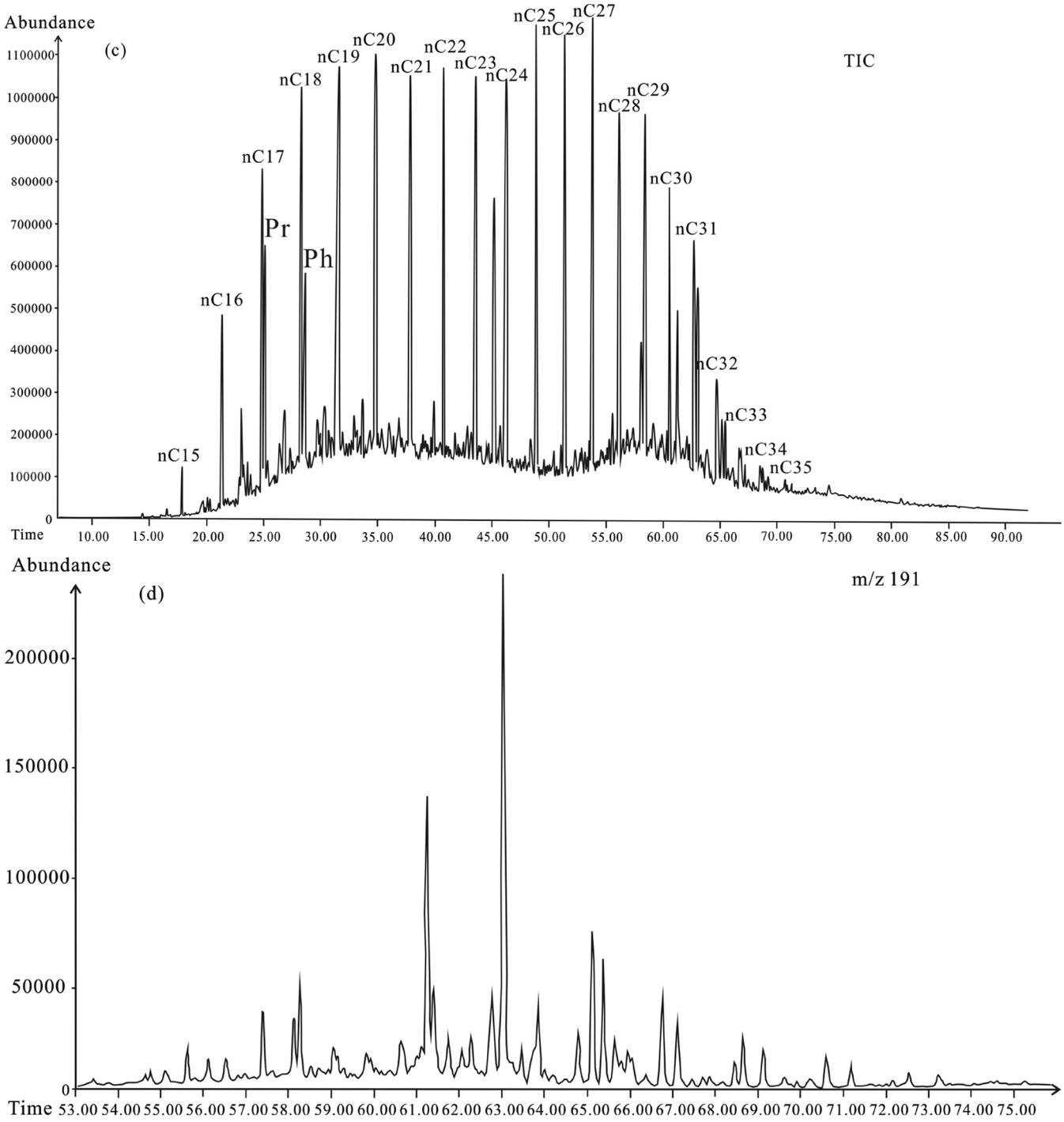

Fig. 4. (*continued*).

samples possess low to high TOC content (0.27–3.59 wt%) with an average of 1.39 wt%. 83.5% of the samples contain organic carbon content greater than 0.5 wt%. This demonstrates that the WC formation is an effective source rock with fair to good generative potential (Table 1 and Fig. 9), which is consistent with Li et al. (2013). Furthermore, the TOC isolines of the Huizhou depression from Shi (2013) showed that the WC has fair to excellent hydrocarbon generation potential (Fig. 10). The amount of hydrocarbon yield (S_2) generated during pyrolysis is a useful indicator of the generation potential of source rocks (Peters, 1986; Bordenave, 1993; Peters and Cassa, 1994). The hydrocarbon yields (S_2) of the samples in this study range from 0.36 to 9.73 mg HC/g rock, with an average of 2.50 mg HC/g rock (Table 2). The hydrocarbon yields (S_2) agree with the TOC content, indicating that the WC formation has fair to good source rock–generative potential (Fig. 11).

5.1.5. Thermal maturity

The thermal maturity of organic matter in the WC formation was evaluated using parameters such as vitrinite reflectance (R_o), pyrolysis T_{max} and production index (PI) (Peters et al., 2005)

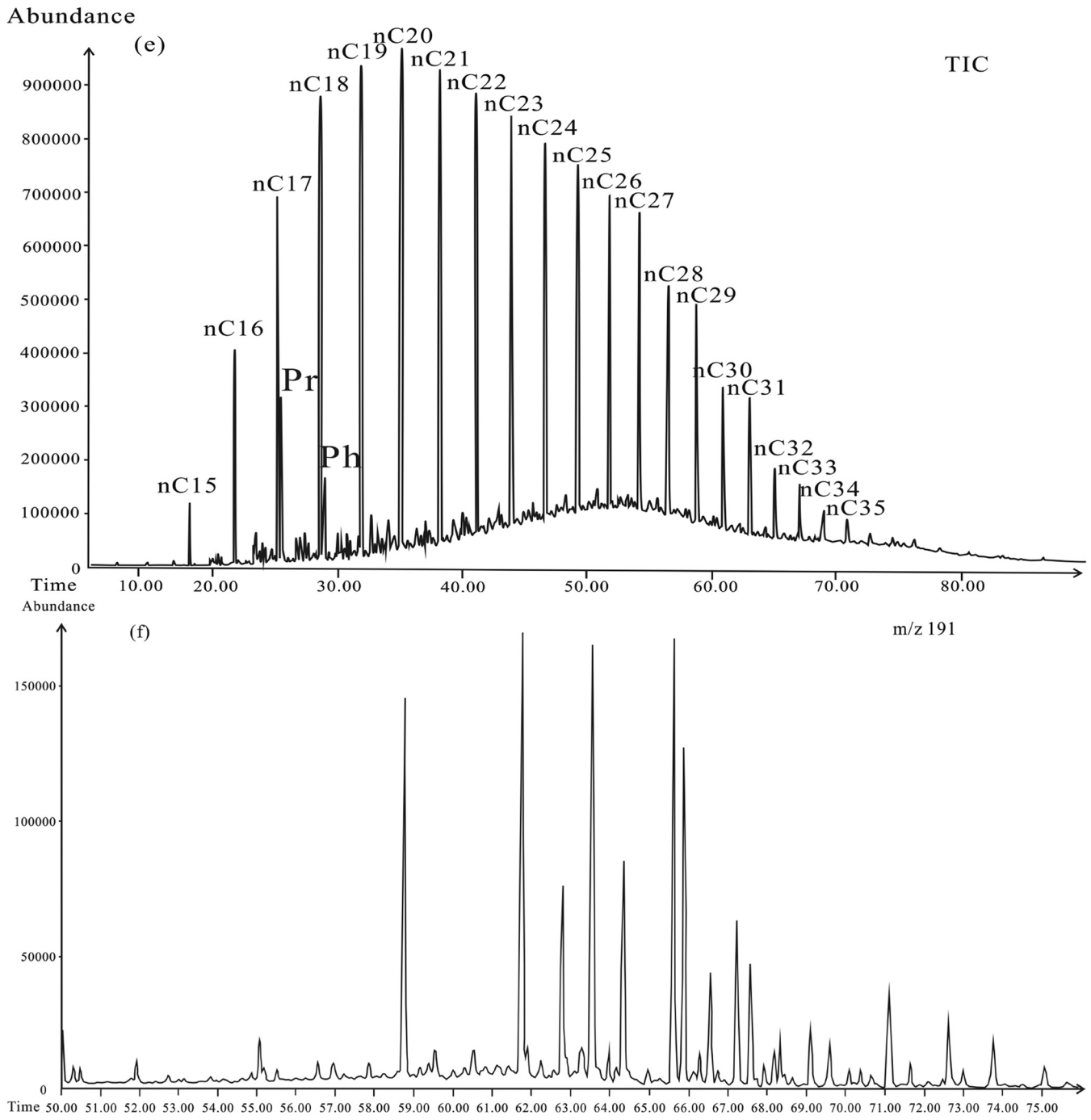

Fig. 4. (*continued*).

Table 4
Biomarker intensities and ratios of the samples in the WC formation, Huizhou depression. (Pr = pristane; Ph = phytane; TAR = Terrigenous Aquatic Ratio).

Well no.	Gammacerane	C30-hopane	Sterane	Hopane	Gammacerane/C30-hopane	Sterane/hopane	Pr/Ph	Pr/nC_{17}	Ph/nC_{18}	TAR
HZ4	262278	1836701	1600545	8670110	0.14	0.18	2.02	0.66	0.31	1.13
HZ5	1341909	11966681	16608886	42678368	0.11	0.39	1.12	0.78	0.57	1.49
HZ6	2928606	76927709	66667881	515955789	0.04	0.13	1.67	0.45	0.21	0.85

(Table 1, Figs. 12 and 13). The thermal maturities for oil and gas generation occur when R_o ranges from 0.5% to 1.0% and from 1.4% to 3.5% respectively, with varying organic matter type (Tissot and Welte, 1984; Espitalié, 1985; Tissot et al., 1987; Bordenave, 1993). Thermogenic oil is often generated when R_o values exceed 0.6% for Type I and Type II kerogen (Bordenave, 1993). This is consistent with the R_o values of the WC samples, which range from 0.656% to 0.781% (Fig. 12).

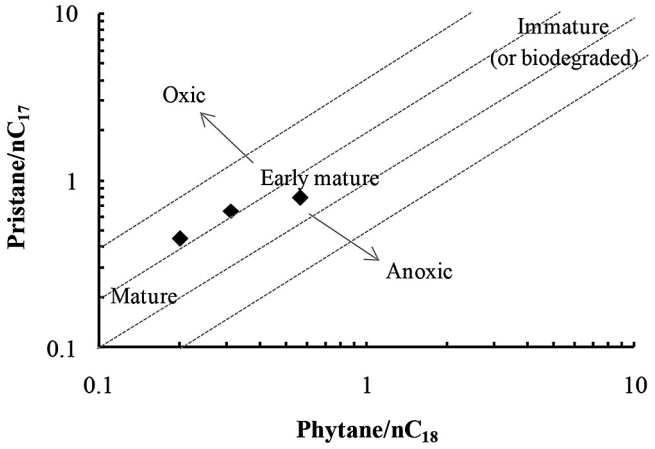

Fig. 5. Plot of Pr/nC17 vs. Ph/nC18 for selected WC samples indicating weak oxidation–weak reduction depositional conditions.

The pyrolysis T_{max} and PI were determined for all the analysed WC samples (Table 1). The WC formation has pyrolysis T_{max} and PI in the range of 419–473 °C and 0.04–0.37 respectively. 66 of the 72 samples are in the main stage of hydrocarbon generation, indicating that most of the WC source rocks are thermally mature (Figs. 8 and 13). Pr/nC_{17} and Ph/nC_{18} ratios plotted in Fig. 5 indicate the WC formation are early mature to mature.

5.2. Hydrocarbon expulsion characteristics of source rocks

5.2.1. Timing of hydrocarbon generation

Thermogenic oil is thought to be generated from source rocks at vitrinite reflectance values between 0.5% and 1.3%, suggest oil-generation window (Tissot and Welte, 1984; Sweeney and Burnham, 1990; Bordenave, 1993), while samples with values less than 0.5% are considered thermally immature. Vitrinite reflectance greater than 1.3% indicates gas window maturity (Tissot and Welte, 1984). The WC source rocks in the Huizhou depression have a TOC value of 0.27–3.59 wt%, with an average of 1.39 wt%, while the maturity ranges from 0.656% to 0.793% R_o, indicating that conditions for hydrocarbon generation and expulsion are present. We constructed the burial history of the HZ1, HZ2 and HZ4 wells (Fig. 1c) using one dimensional basin modelling (Sweeney and Burnham, 1990) with the depositional age, thickness, and erosion for the formations, which are penetrated by the studied wells (Table 2). The burial history of the studied wells is very similar (Fig. 14), and these similar burial histories should produce a much more similar observed maturity profile with the same regional heat flow history studied by Shi et al., 2003. Subsequently, we inferred the thermal history of the WC formation in the HZ1, HZ2 and HZ4 wells together with the burial history we constructed, measured R_o and geothermal gradient data from well drilling repots (Figs. 14 and 15). There is a good match between optically measured (symbols) and calculated (lines) vitrinite reflectance (R_o) (Fig. 15). This calibration data helped us to reconstruct and validate the thermal history in the study area. The detailed maturity history of WC source rocks for the representative wells HZ1, HZ2 and HZ4 helps us to determine the time when source rocks passed through the oil window. According to the vitrinite reflectance (% Ro) data and its best-fit calibration with the calculated maturity in the one-dimensional model (Fig. 15), the WC formation became mature in the Middle Miocene, when the temperature of the WC formation increased to approximately 80–90 °C and the vitrinite reflectance (R_o) increased to approximately 0.5%, at the depth of 2300–2500 m (Fig. 13). Since the middle Miocene, the thermal maturity gradually increased, with the formation temperature increasing from 80 to 90 °C to more than 120 °C and the thermal maturity evolving from 0.5% to 1.0% R_o. The source rocks were in the mature stage with large amounts of oil generated since the middle Miocene. Using the combined information from core samples, one dimensional burial history simulations and the structural isoline of the WC formation, we constructed a present vitrinite reflectance (R_o) distribution map for the WC formation (Fig. 16). The inferred thermal maturity is controlled by the tectonic framework in the depression. On the margins of the depression in the southwest of the study area, the source rocks are mature to highly mature with R_o from 0.6% to 1.2% and large oil generation amounts. Correspondingly, the source rocks in the centre of each sag are mainly highly mature to post mature, with R_o from 1.2% to 2.1% and gas generation at present (Fig. 16).

5.2.2. Hydrocarbon expulsion model

The hydrocarbon generation threshold in the Huizhou depression is 0.5% R_o, which is consistent with previous studies (e.g. Tissot and Welte, 1984; Tissot et al., 1987) (Fig. 17a). The hydrocarbon expulsion threshold is 0.8% R_o, and the original hydrocarbon generation potential index (GPI_o) of the WC source rocks is 380 mg HC/g TOC (Fig. 17a). Once the hydrocarbon expulsion threshold was reached, the residual hydrocarbon generation potential index, as measured from the samples, decreased. The measured GPI_r can be calculated using Eq. (10). Then, the restoration coefficient, the real residual hydrocarbon generation potential index (GPI_{ro}), the hydrocarbon expulsion capacity (q_{he}) and the hydrocarbon expulsion rate (r_{he}) can be calculated and expressed using Eqs. (11)–(14), respectively. The hydrocarbon expulsion capacity (q_{he}) increased rapidly in the early period and then slowed in the later stage (Fig. 17b). The expulsion peak, at which the hydrocarbon expulsion rate was the greatest, occurred at 1.1% R_o (Fig. 17c). As the degree of thermal evolution of source rocks increases, the hydrocarbon expulsion efficiency, which is the percentage of hydrocarbon expulsion to the maximum hydrocarbon generation potential, increases from 0 to 75% (Fig. 17d).

$$GPI_r = 504.5e^{-\left(\frac{R_o-0.2499}{1.078}\right)^2}, \quad R_o \geq 0.8 \qquad (10)$$
$$R^2 = 0.9748$$

$$k = 1.303 - 0.546e^{-\left(\frac{R_o-0.2499}{1.078}\right)^2} \qquad (11)$$

$$GPI_{ro} = \frac{GPI_r}{k} = \frac{504.5e^{-\left(\frac{R_o-0.2499}{1.078}\right)^2}}{1.303 - 0.546e^{-\left(\frac{R_o-0.2499}{1.078}\right)^2}} \qquad (12)$$

$$q_{he} = GPI_o - GPI_{ro} = 380 - \frac{504.5e^{-\left(\frac{R_o-0.2499}{1.078}\right)^2}}{1.303 - 0.546e^{-\left(\frac{R_o-0.2499}{1.078}\right)^2}} \qquad (13)$$

$$r_{he} = \frac{dq_{he}}{dR_o} = \frac{1148.34(R_o - 0.2499)e^{-\left(\frac{R_o-0.2499}{1.078}\right)^2}}{\left[1.303 - 0.546e^{-\left(\frac{R_o-0.2499}{1.078}\right)^2}\right]^2} \qquad (14)$$

where, GPI_r is the remaining hydrocarbon generation potential index (mg HC/g TOC); PGI_o is the hydrocarbon generation potential

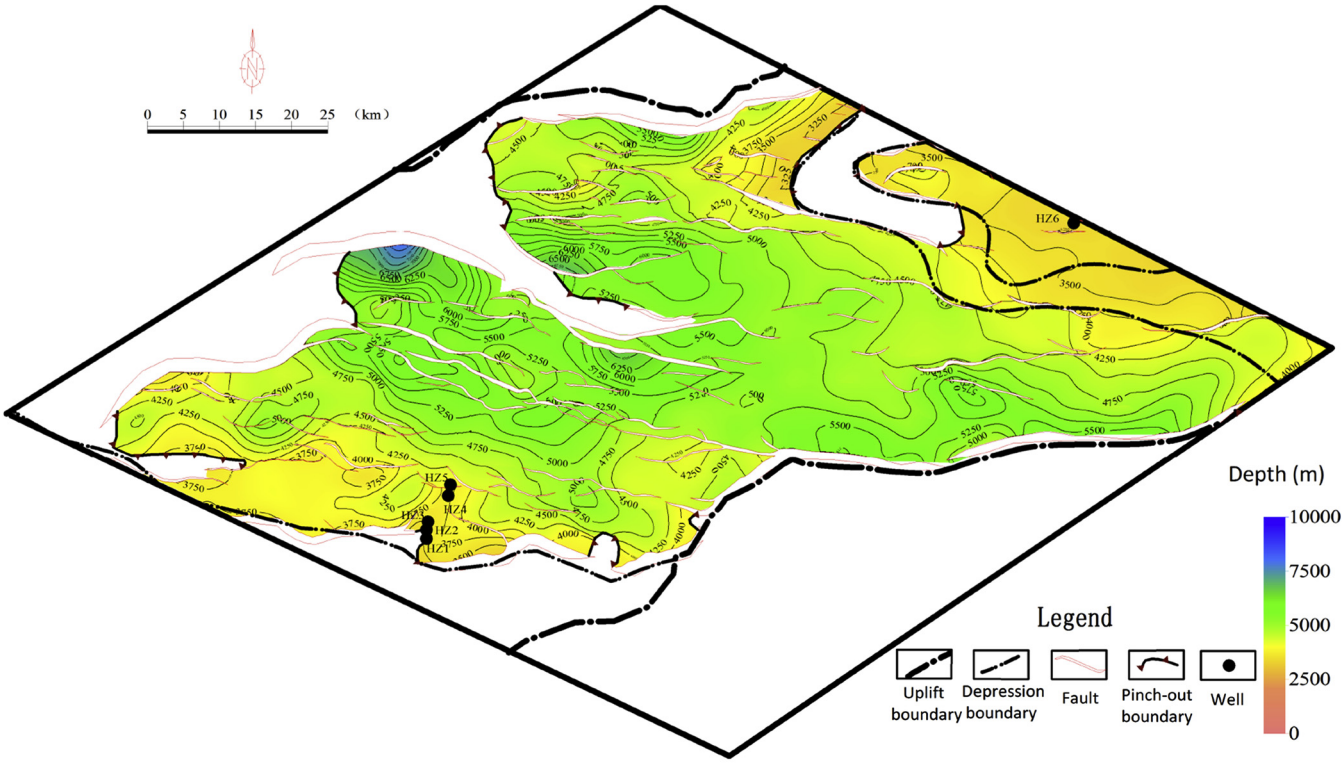

(a)

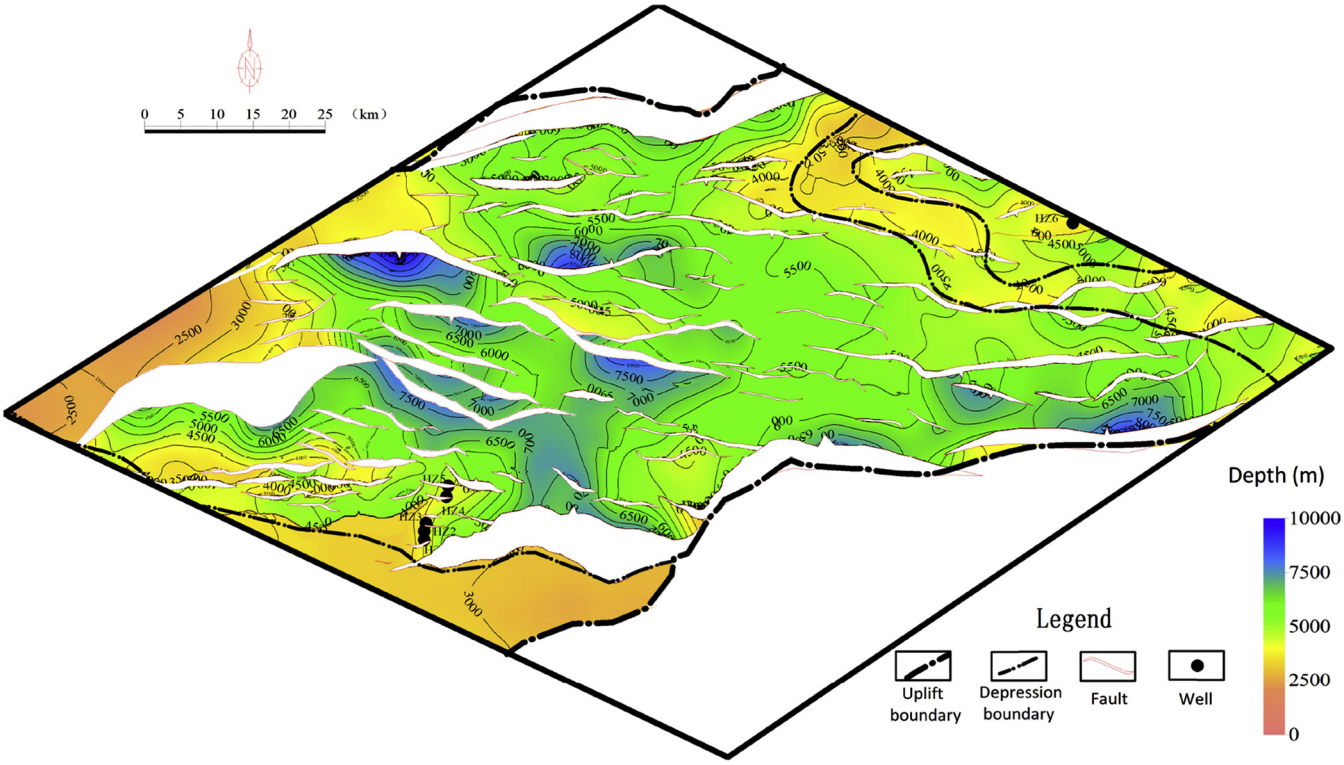

(b)

Fig. 6. Coutour map of (a) top and (b) bottom of the WC formation.

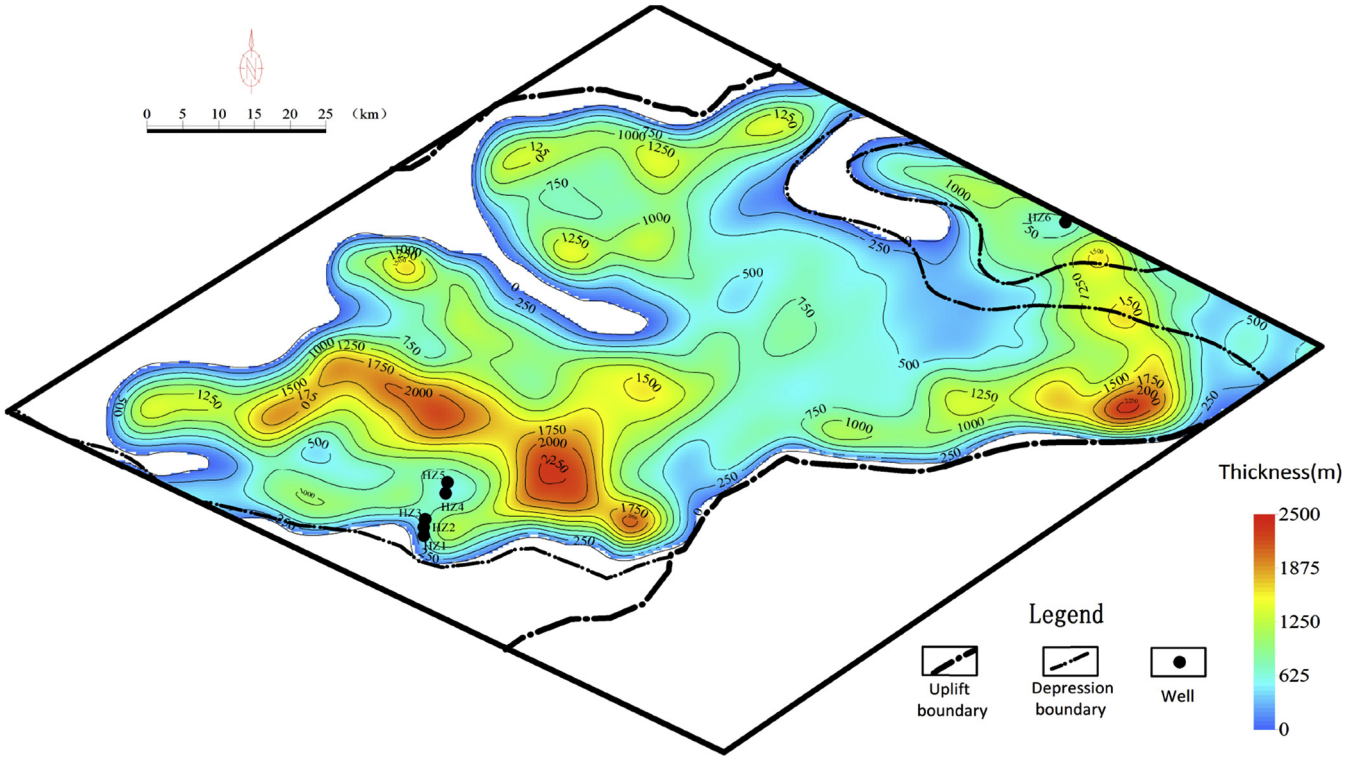

Fig. 7. The isopach map of WC formation in the Huizhou depression.

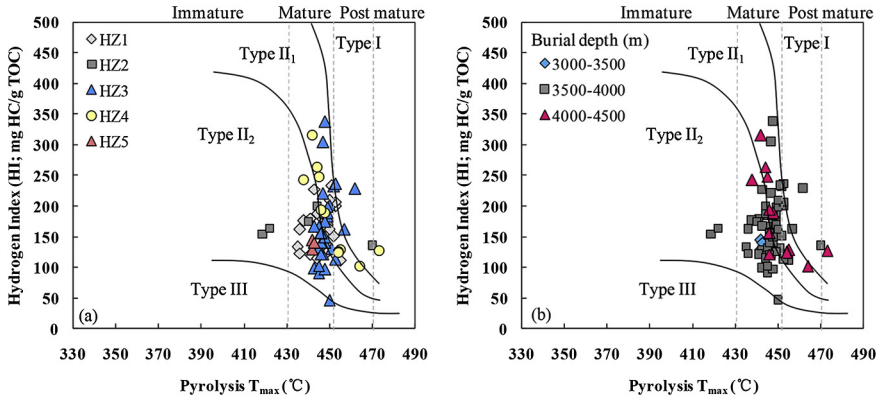

Fig. 8. Plot of Hydrogen Index (HI) versus pyrolysis T_{max} (a) according to the well and (b) according to the depth, showing kerogen quality and thermal maturity stages of the WC formation.

index at the expulsion threshold (mg HC/g TOC); R_o is vitrinite reflectance (%); k is the restoration coefficient; GPI_{ro} is the real residual hydrocarbon generation potential index (mg HC/g TOC); q_{he} is the hydrocarbon expulsion capacity (mg HC/g TOC); r_{he} is the hydrocarbon expulsion rate (mg HC/g TOC).

5.2.3. Hydrocarbon expulsion intensity and amount

The regional hydrocarbon expulsion intensities were calculated using Eqs. (4) and (5) and the regional variations of the source rock characteristics and thermal maturity illustrated previously (Figs. 7–17). Thermally mature source rocks occur mainly in the structural sags, including the H26 sag, X24 sag, H21 sag, H08 sag and H10 sag (Fig. 18). The calculated maps indicate that all the WC source rocks have reached the expulsion threshold, with seven hydrocarbon expulsion centres (the H26 sag, H21 sag, X24 sag, X23 sag, H08 sag, H14 sag and H24 sag). The greatest hydrocarbon expulsion intensity, 104×10^6 t/km^2, occurs in the H26 Sag (Fig. 18). The expulsion intensities in the H21 sag, X24 sag, X23 sag are lower, with their respective greatest expulsion intensities being 71×10^6, 62×10^6 and 53×10^6 t/km^2.

The differences in hydrocarbon expulsion intensity are controlled by the combination of thermal maturation, thickness and organic matter abundance in the WC source rock formation. The cumulative amounts of hydrocarbon expulsion were obtained by integrating the hydrocarbon expulsion intensity curves (Eq. (9)). The total expelled hydrocarbon quantities are 690.1×10^8 t.

5.3. Significance for hydrocarbon accumulation

The geological and geochemical characteristics of the WC source rocks in the Huizhou depression were investigated, and an improved mass balance approach was proposed to evaluate the

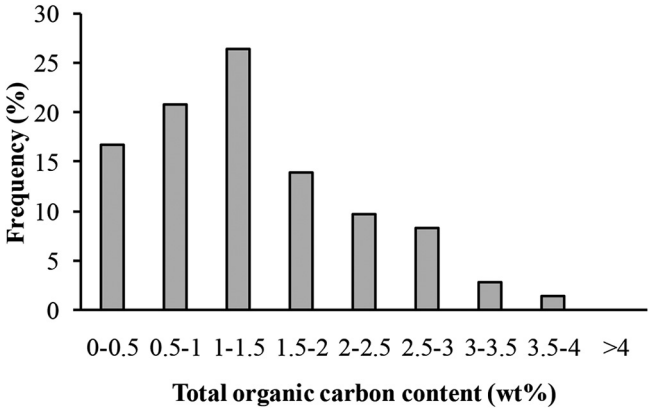

Fig. 9. Histogram showing the TOC contents of WC source rocks.

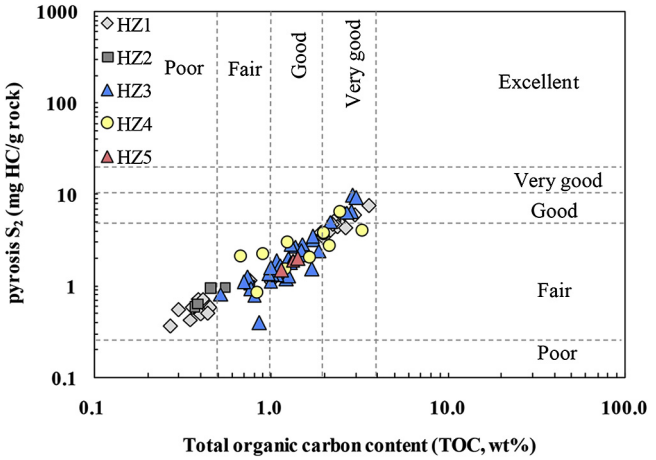

Fig. 11. Pyrosis S_2 versus Total organic carbon (TOC) plot showing generative source rock potential for the WC formation in the Huizhou depression.

hydrocarbon expulsion intensity and amounts in this article. Oils are discovered in the WC formation of the HZ3 well during the exploration with flow rate of 26 m^3/d, which was collected from the well drilling report from the China National Offshore Oil Corporation Limited-Shenzhen. This indicates that the WC formation has favourable source potential for hydrocarbon accumulation. This kind of self generation-self accumulation resource maybe largely distributed, especially in the centre of the depression. Besides, all the wells in this study are located on the margins of sags (Fig. 1c) and thus, parameters of the WC source rocks (e.g. thickness) are underestimated. Compared with the calculated volumetric result, the real hydrocarbon resources may be much larger. In summary, WC formation has great potential for hydrocarbon generation and expulsion. Hydrocarbon accumulations can occur without long distance for migration, forming unconventional resources (e. g. tight oil, shale oil). It makes the WC formation the main exploration target in the future, without the economic consideration.

6. Conclusions

A conventional and systematic evaluation of the WC source rocks in the Huizhou depression, Pearl River Mouth basin (PRMB) was conducted for the first time. The WC source rocks are widely distributed, with a large thickness (mostly thicker than 200 m, with a maximum thickness greater than 1000 m) and were deposited in a lacustrine weak oxidation–weak reduction sedimentary environment with low salinity. The source rocks have low to high

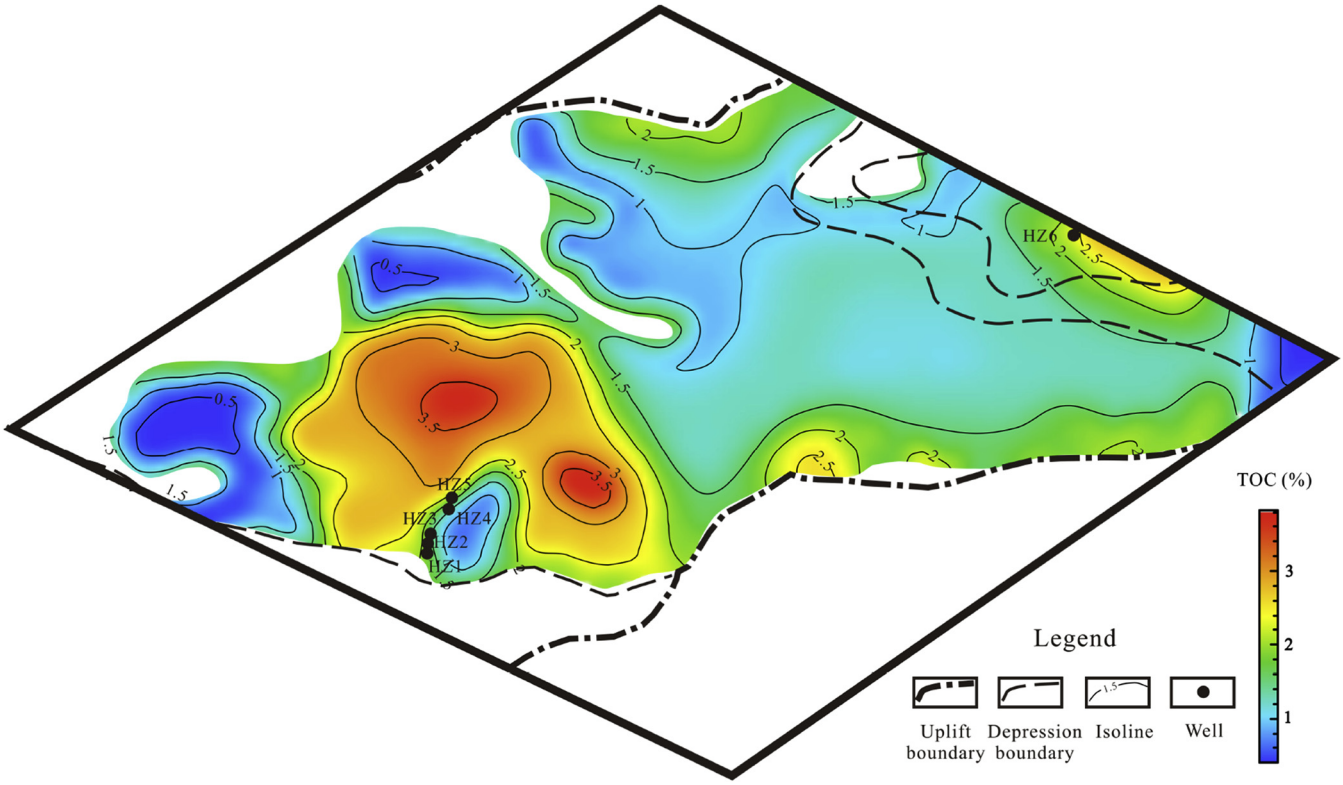

Fig. 10. Coutour map of TOC distribution of WC formation in the Huizhou depression, Pearl River Mouth Basin (contour values in wt.%) (after Shi, 2013).

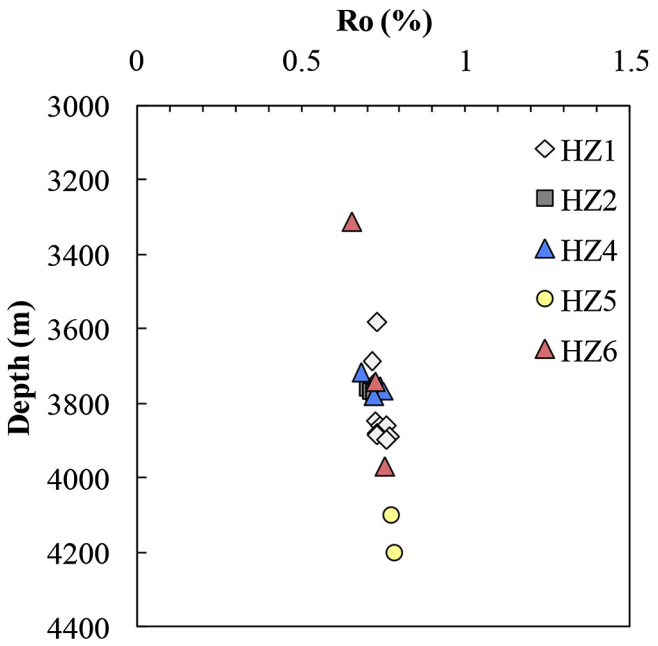

Fig. 12. Plot of vitrinite reflectance (R_o) versus burial depth.

organic matter abundance (TOC mainly ranges from 0.27 to 3.59 wt %, with an average of 1.39 wt%) dominated by II_1–type and II_2–type kerogen, resulting in significant hydrocarbon generating strength under middle–high thermal evolution (R_o mainly ranges from 0.65% to 1.2% on the margins of sags and greater than 1.2% in the centre of sags). All the results show that the WC source rocks have significant hydrocarbon generation potential.

The hydrocarbon generation timing of the WC source rocks was evaluated by one dimensional basin modelling using data from the HZ1, HZ2 and HZ4 wells. The hydrocarbon expulsion characteristics including expulsion intensity, efficiency and quantities were investigated using an improved hydrocarbon generation potential methodology. The results indicate that the source rocks became mature (R_o = 0.5%) in the early Miocene and began to generate hydrocarbons. They reached the hydrocarbon expulsion threshold at 0.8% R_o and the hydrocarbon expulsion rate was the greatest at 1.1% R_o. The expulsion intensities in the H26 sag, H21 sag, X24 sag and X23 sag are relatively large, with their respective greatest expulsion intensities being 104 × 10^6, 71 × 10^6, 62 × 10^6 and 53 × 10^6 t/km^2. The comprehensive hydrocarbon expulsion

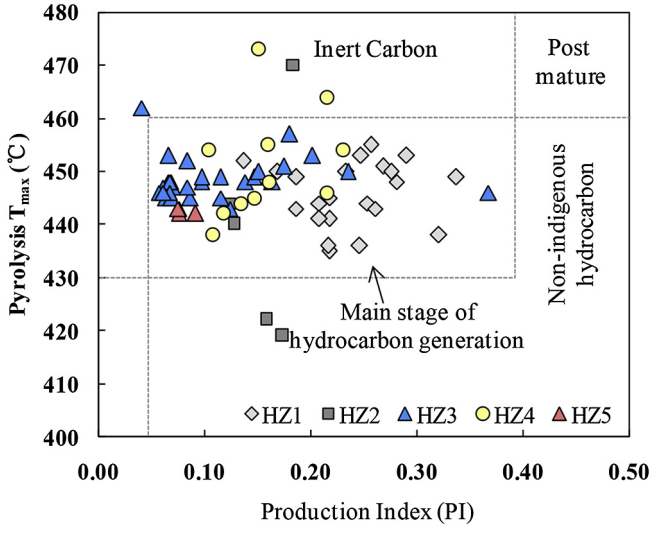

Fig. 13. Plot of pyrolysis T_{max} versus production index (PI), showing the maturation and nature of the hydrocarbon products of the WC formation.

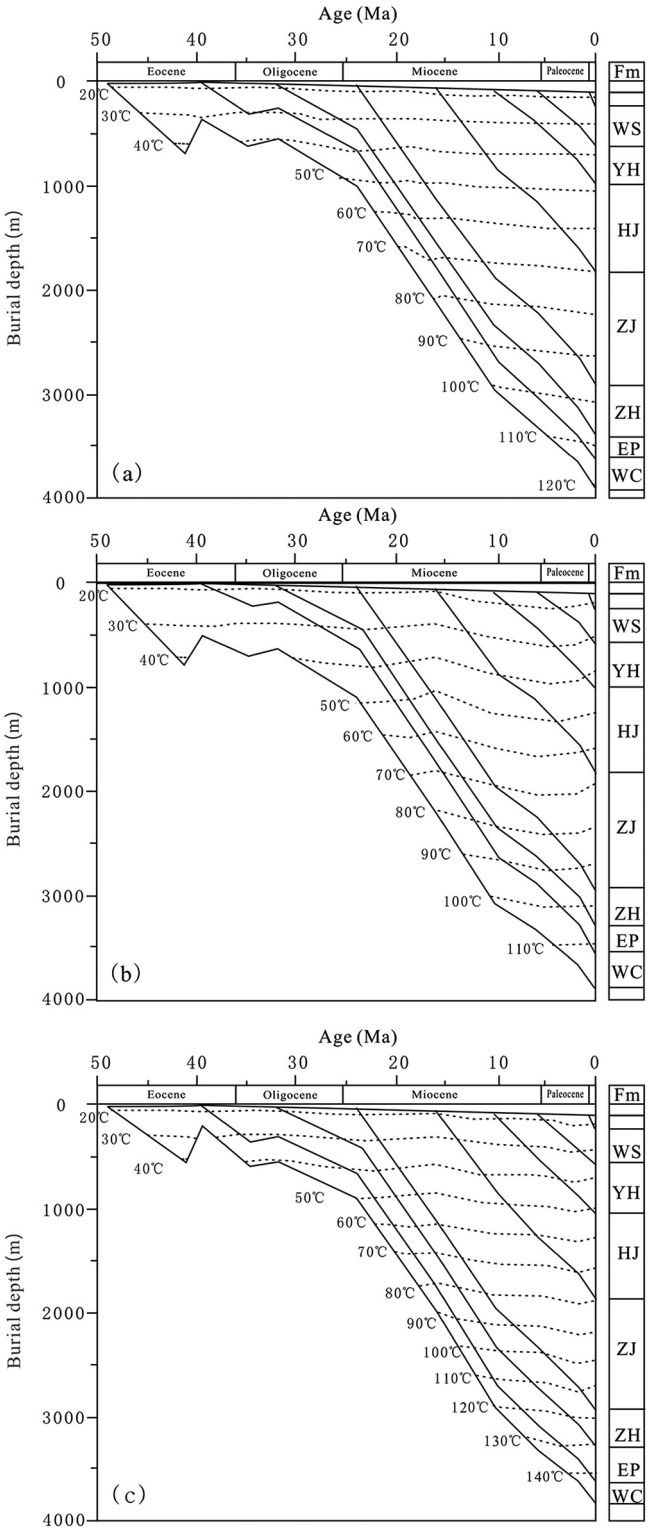

Fig. 14. Burial history by one dimensional basin modelling of the WC source rocks in the Huizhou depression (a. HZ1 well; b. HZ2well; c. HZ4 well).

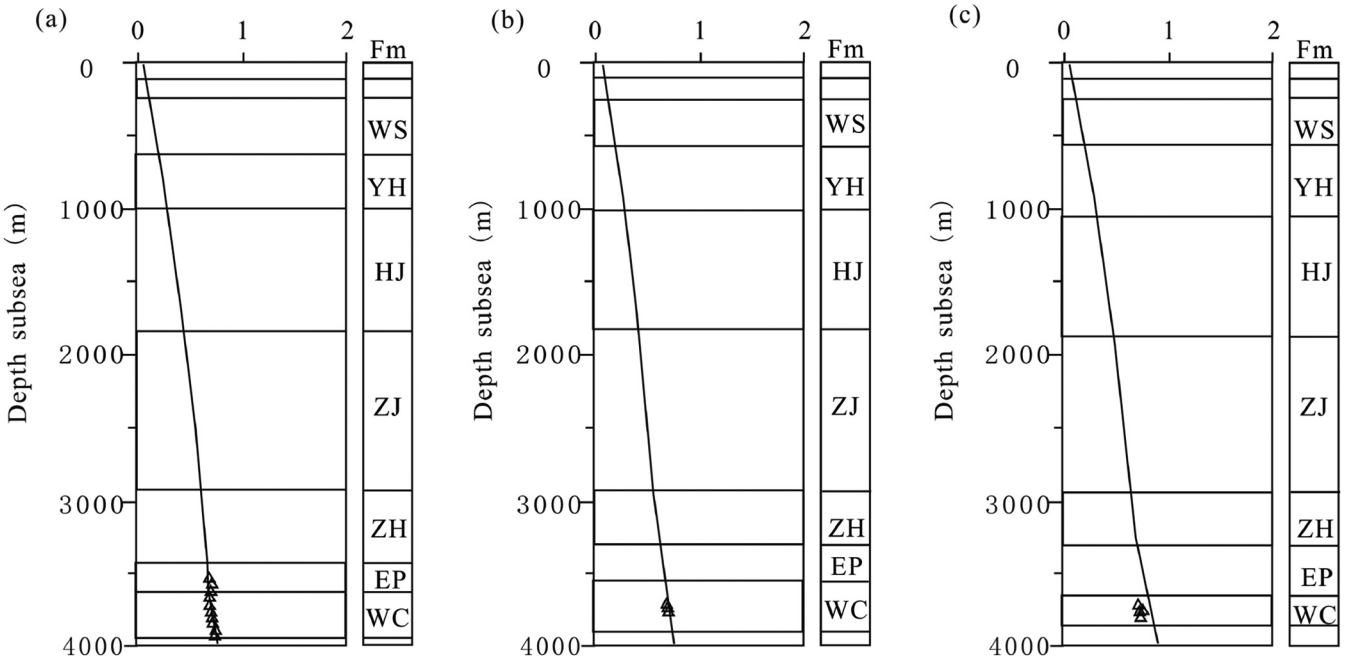

Fig. 15. Vitrinite reflectance evolution by one dimensional basin modelling of the WC source rocks in the Huizhou depression (a. HZ1 well; b. HZ2well; c. HZ4 well).

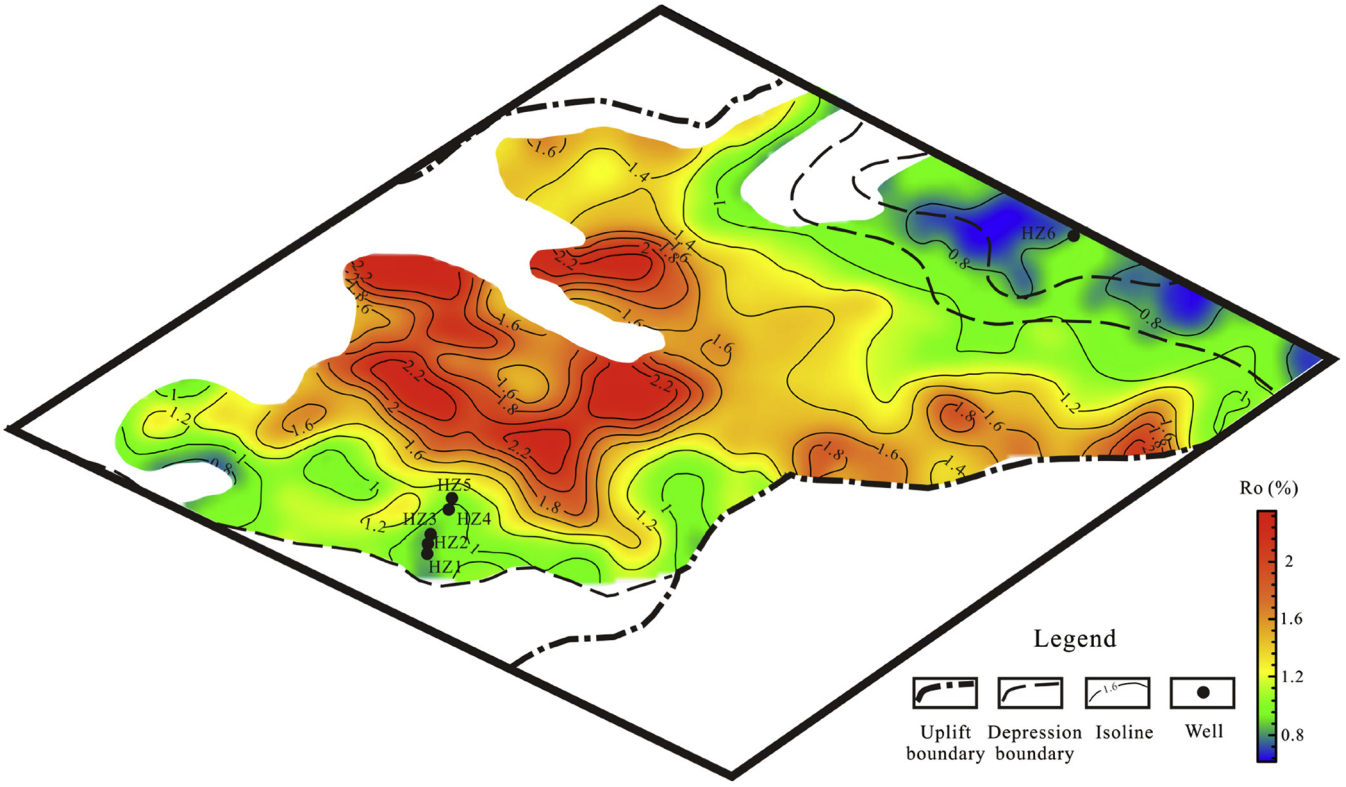

Fig. 16. R_o distribution of the WC formation in the Huizhou depression, PRMB (contour values in %).

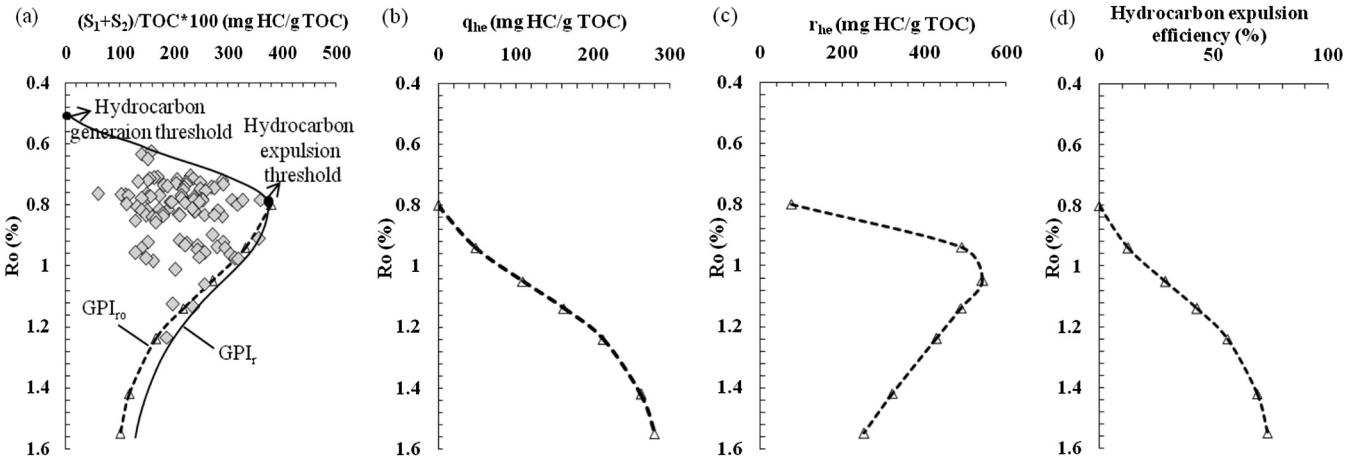

Fig. 17. Operational model for the quantification of hydrocarbon generation and expulsion of the WC source rocks in the Huizhou depression.

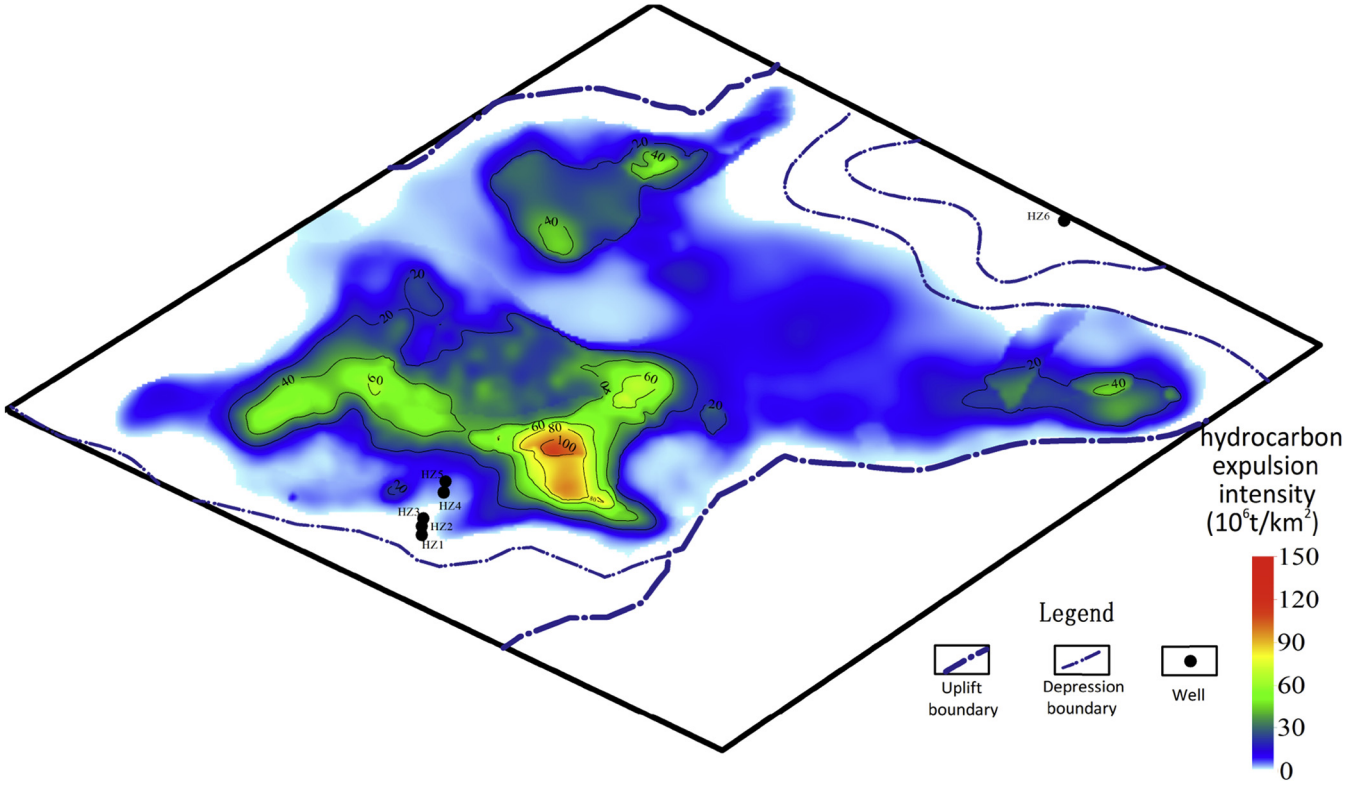

Fig. 18. Recent hydrocarbon expulsion intensity of WC source rocks in the Huizhou depression (contour values in $\times$ 10^6 t/km^2).

efficiency was approximately 75%. The hydrocarbon quantities expulsed from the WC source rocks are 690.1 $\times$ 10^8 t.

Acknowledgements

This study was funded by the National Major Scientific and Technological Special Project during the Twelfth Five-year Plan Period (Grants No. 2011ZX05023-006-003 and CNOOC-KJ125ZDXM07). We would like to express our gratitude to the China National Offshore Oil Corporation (CNOOC) for providing basic data and permitting publishing of the results. The insightful reviews by Editor Daniel S. Alessi and the anonymous reviewers significantly improved the manuscript, for which we are grateful.

References

Aali, J., Rahmani, O., 2011. Evidences for secondary cracking of oil in South Pars field, Persian Gulf, Iran. J. Petrol. Sci. Eng. 76, 85–92.
Allen, P.A., Allen, J.R., 1990. Basin Analysis Principles and Applications. Blackwell Scientific Publications, Oxford, pp. 1–642.
Amane, W., Hideki, N., 1997. Geochemical characteristics of terrigenous and marine sourced oils in Hokkaido, Japan. Org. Geochem. 28, 27–41.
Aquilera, C.L., Huizinga, B.J., Lomando, A.J., 1990. Petroleum geology of the zhu 1 depression, Pearl River mouth basin, People's Republic of China. Am. Assoc. Pet. Geol. Bull. 74, 596 (abstract).
Bordenave, M.L., 1993. Applied Petroleum Geochemistry. Editions Technip, Paris.
Bou Daher, S., Nader, F.H., Müller, C., Littke, R., 2015. Geochemical and petrographic characterization of campaniane-lower maastrichtian calcareous petroleum source rocks of Hasbayya, South Lebanon. Mar. Pet. Geol. 64, 304–323.
Burnham, A.K., 1989. On the validity of the pristane formation index. Geochim. Cosmochim. Acta 53, 1693–1697.

Chen, C.M., 2000. Petroleum geology and conditions for hydrocarbon accumulation in the Eastern Pearl River Mouth Basin. China Offshore Oil Gas (Geology) 14, 73–82 (in Chinese with English abstract).
Chen, S., Pei, C., 1993. Geology and geochemistry of source rocks of the Eastern Pearl River Mouth basin, South China Sea. J. Southeast Asian Earth Sci. 8, 393–406.
Cheng, P., Tian, H., Huang, B.J., Wilkins, R.W.T., Xiao, X.M., 2013. Tracing early–-charged oils and exploration directions for the Wenchang A sag, western Pearl River Mouth Basin, offshore South China Sea. Org. Geochem 61, 15–26.
Cui, S.S., He, J.X., Chen, S.H., Zou, H.P., Cui, J., 2009. Development characteristics of Pearl River mouth basin and its geological conditions for oil and gas accumulation. Nat. Gas. Geosci. 20, 384–391 (in Chinese with English abstract).
Espitalié, J., 1985. Use of T_{max} as a maturation index for different types of organic matter–comparison with vitrinite reflectance. In: Burrus, J. (Ed.), Thermal Modeling in Sedimentary Basins. Editions Technip, Paris, pp. 475–496.
Espitalié, J., Laporte, L.J., Madec, M., Marquis, F., Leplat, P.J., Boutefeu, A., 1977. Méthode rapide de caractérisation des roches méres de leur potential petrolier et de leur degré d'évolution. Rev. Inst. Franc. Pet. 32, 23–42.
Fu, N., Li, Y.C., Wang, J.R., 2001. Oil–source correlation in the western Huizhou Sag. China Offshore Oil Gas (Geology) 15 (5), 322–327 (in Chinese with English abstract).
Gong, Z.S., Li, S.T., 2004. Dynamic Research of Oil and Gas Accumulation in Northern Marginal Basins of South China Sea. Science Press, Beijing (in Chinese).
Guo, B.J., Xie, J.S., Xiang, F.D., 2000. The study of the petroleum system in the Zhu 1 depression in Pearl River Mouth Basin. China Offshore Oil Gas (Geology) 14, 1–8 (in Chinese with English abstract).
Guo, J.G., Pang, X.Q., Guo, F.T., Wang, X.L., Xiang, C.F., Jiang, F.J., Peng, W.L., Xu, J., Hu, T., Wang, P.W., 2014. Petroleum generation and expulsion characteristics of Lower and Middle Jurassic source rocks on the southern margin of Junggar Basin, northwest China: implications for unconventional gas potential. Can. J. Earth Sci. 51, 537–557.
Hakimi, M.H., Abdullah, W.H., 2015. Thermal maturity history and petroleum generation modelling for the Upper Jurassic Madbi source rocks in the Marib-Shabowah Basin, western Yemen. Mar. Pet. Geol. 59, 202–216.
Hakimi, M.H., Shalaby, M.R., Abdullah, W.H., 2012a. Molecular composition and organic petrographic characterization of Madbi source rocks from the Kharir oilfield of the Masila Basin (Yemen): palaeoenvironmental and maturity interpretation. Arab. J. Geosci. 5, 817–831.
Hakimi, M.H., Shalaby, M.R., Abdullah, W.H., 2012b. Geochemical and petrographic characterization of organic matter in the Upper Jurassic Madbi shale succession (Masila Basin, Yemen): origin, type and preservation. Org. Geochem 49, 18–29.
Hakimi, M.H., Abdullah, W.H., Sia, S.G., Makeen, Y.M., 2013. Organic geochemical and petrographic characteristics of Tertiary coals in the northwest Sarawak, Malaysia: Implications for palaeoenvironmental conditions and hydrocarbon generation potential. Mar. Pet. Geol. 48, 31–46.
Lee, Y.J., 1997. Geochemical characteristics of organic matter in the tertiary sediments from the JDZ Blocks, offshore Korea. Korean J. Petrol. Geol. 6, 25–36.
Li, M.W., Zhang, S.C., Snowdon, L., Issler, D., 2008. Oil–source correlation in tertiary deltaic petroleum systems: a comparative study of the Beaufort–Mackenzie Basin in Canada and the Pearl River Mouth Basin in China. Org. Geochem 39, 1170–1175.
Li, S.F., Xu, S.H., Shi, H.S., Mei, L.F., Shu, Y., Cao, T.T., 2013. Characteristics of Paleogene source rocks and prediction of petroleum resources in Huizhou depression, Pearl River Mouth basin. Earth Science–Journal China Univ. Geosci. 38, 112–120 (in Chinese with English abstract).
Mukhopadhyay, P.K., Wade, J.A., Kruge, M.A., 1995. Organic facies and maturation of Jurassic/Cretaceous rocks, and possible oil–source rock correlation based on pyrolysis of asphaltenes, Scotion Basin, Canada. Org. Geochem 22, 85–104.
Nicholas, B.H., Katherine, H.F., Richard, D.P., Timothy, S.W., Gareth, D.M., 2004. The character and origin of lacustrine source rocks in the Lower Cretaceous synrift section, Congo Basin, West Africa. Am. Assoc. Pet. Geol. Bull. 88, 1163–1184.
Nie, F.J., Li, S.T., Wang, H., Xie, X.N., Wu, K.Q., Jiang, M.Z., 2001. Lateral migration pathways of petroleum in the Zhu III subbasin, Pearl River Mouth basin, South China Sea. Mar. Pet. Geol. 18, 561–575.
Obermajer, M., Dewing, K., Fowler, M.G., 2010. Geochemistry of crude oil from Bent Horn field (Canadian Arctic Archipelago) and its possible Paleozoic origin. Org. Geochem 41, 986–996.
Oppo, D., Capozzi, R., Picotti, V., 2013. A new model of the petroleum system in the Northern Apennines, Italy. Mar. Pet. Geol. 48, 57–76. http://dx.doi.org/10.1016/j.marpetgeo.2013.06.005.
Pang, X.Q., Li, M.W., Li, S.M., Jin, Z.J., 2005. Geochemistry of petroleum systems in the Niuzhuang South Slope of Bohai Bay Basin: Part 3. Estimating petroleum expulsion from the Shahejie formation. Org. Geochem. 36, 497–510.
Peters, K.E., 1986. Guidelines of evaluating petroleum source rock using programmed pyrolysis. Am. Assoc. Pet. Geol. Bull. 70, 318–329.
Peters, K.E., Cassa, M.R., 1994. Applied source rock geochemistry. In: Magoon, L.B., Dow, W.G. (Eds.), The Petroleum System D from Source to Trap, Am. Assoc. Pet. Geol., Memoir, 60, pp. 93–120.
Peters, K.E., Moldowan, J.M., 1993. The Biomarker Guide: Interpreting Molecular Fossils in Petroleum and Ancient Sediments. Prentice Hall, Englewood Cliffs.
Peters, K., Fraser, T., Amris, W., Rustanto, B., 1999. Geochemistry of crude oils from eastern Indonesia. Am. Assoc. Pet. Geol. Bull. 83, 1927–1942.
Peters, K.E., Walters, C.C., Moldowan, J.M., 2005. The Biomarker Guide: Biomarkers and Isotopes in Petroleum Exploration and Earth History, second ed. Cambridge University Press, Cambridge, UK.
Powell, T.G., 1988. Pristane/phytane ratio as environmental indicator. Nature 333, 604.
Powell, T.G., McKirdy, D.M., 1973. Relationship between ratio of pristane to phytane, crude oil composition and geological environment in Australia. Nat. Phys. Sci. 243, 37–39.
Robison, C.R., Elrod, L.W., Bissada, K.K., 1998. Petroleum generation, migration, and entrapment in the Zhu 1 depression, Pearl River Mouth basin, South China Sea. Int. J. Coal Geology 37, 155–178.
Shi, H.S., 2013. On heterogeneous distribution and differential enrichment by zones of hydrocarbon resources: a case in Zhu I depression, Pearl River Mouth basin. China Offshore Oil Gas 25 (1–8), 25 (in Chinese with English abstract).
Shi, X.B., Qiu, X.L., Xia, K.Y., Zhou, D., 2003. Characteristics of surface heat flow in the South China Sea. J. Asian Earth Sci. 22 (3), 265–277.
Shi, H.S., Yu, S.M., Mei, L.F., Shu, Y., Wu, J.Y., 2009. Features of Paleogene episodic rifting in Huizhou fault depression in the Pearl River Mouth Basin. Nat. Gas. Ind. 29, 35–40 (in Chinese with English abstract).
Sinninghe Damsté, J.S., Kenig, F., Koopmans, M.P., Köster, J., Schouten, S., Hayes, J.M., de Leeuw, J.W., 1995. Evidence for gammacerane as an indicator of water column stratification. Geochimica Cosmochimica Acta 59, 1895–1900.
Sun, Q.L., Wu, S.G., Cartwright, J., Dong, D.D., 2012. Shallow gas and focused fluid flow systems in the Pearl River Mouth Basin, northern South China Sea. Mar. Geol. 315–318, 1–14.
Sweeney, J.J., Burnham, A.K., 1990. Evaluation of a simple model of vitrinite reflectance based on chemical kinetics. Am. Assoc. Pet. Geol. Bull. 74, 1559–1570.
Tissot, B.P., Welte, D.H., 1984. Petroleum Formation and Occurrence. Springer–Verlag, New York, p. 699.
Tissot, B.P., Pelet, R., Ungerer, P.H., 1987. Thermal history of sedimentary basins, maturation indices, and kinetics of oil and gas generation. Am. Assoc. Pet. Geol. Bull. 71, 1445–1466.
Volkman, J.K., Maxwell, J.R., 1986. Acyclic isoprenoids as biological markers. In: Johns, R.B. (Ed.), Biological Markers in the Sedimentary Record. Elsevier, New York.
Wang, C.X., Zhang, Q.Y., 1999. Typical oil and gas reservoirs and their forming conditions in the Zhu III sag. China Offshore Oil Gas (Geology) 13, 248–238 (in Chinese with English Abstract).
Waples, D.W., 1985. Geochemistry in Petroleum Exploration. Reidel, Boston, USA, p. 232.
Wu, J., Ye, J.R., Shi, H.S., Shu, Y., Kang, J.Y., 2012. Reservoir–forming pattern of typical hydrocarbon accumulation zone in huizhou sag. J. Southwest Petroleum Univ. Sci. Technol. Ed. 34, 17–26 (in Chinese with English Abstract).
Wu, Q.Q., Ye, J.R., Shi, H.S., Shu, Y., Wu, J., 2013. Hydrocarbon accumulation process in western Huizhou sag. J. Northeast Petrol. Univ. 37, 32–42 (in Chinese with English abstract).
Xu, S.H., Li, S.F., Yuan, C.P., 2012. Resource potential of water-soluble gas in the Palaeogene huizhou sag, Pearl River mouth Basin. Petrol. Explor. Dev. 39, 194–201.
Yuan, C.P., Xu, S.H., Xue, L., 2014. Prediction and evaluation with logging of main source rocks in Huizhou Sag, Pearl River Mouth Basin. Petrol. Geol. Exp. 36, 110–116 (in Chinese with English abstract).
Zhang, S.C., Liang, D.G., Gong, Z.S., Wu, K.Q., Li, M.W., Song, F.Q., Song, Z.G., Zhang, D.J., Wang, P.R., 2003. Geochemistry of petroleum systems in the eastern Pearl River Mouth Basin: evidence for mixed oils. Org. Geochem. 34, 971–991.
Zhang, C.M., Li, S.T., Yang, J.M., Yang, K., Wang, J.R., 2004. Petroleum migration and mixing in the Pearl River mouth basin, South China sea. Mar. Pet. Geol. 21, 215–224.
Zhong, N.N., Lu, S.F., Huang, Z.L., Xue, H.T., 2004. An approach to the evolution of TOC value for source rock and its relation to efficiencies of hydrocarbon genera ion and expulsion. Acta Sedimentol. Sin. 22 (Suppl. l), 73–78 (in Chinese with English abstract).
Zhou, Z.Y., 2009. Quantitative analysis of variation of organic carbon mass and content in source rock during evolution process. Petrol. Explor. Dev. 36, 463–468.
Zhou, J., Pang, X.Q., 2002. A method for calculating the quantity of petroleum generation and expulsion. Petrol. Explor. Dev. 29, 24–27.
Zhou, D., Zhao, Z.X., Liao, J., Sun, Z., 2011. A preliminary assessment on CO2 storage capacity in the Pearl River Mouth Basin offshore Guangdong, China. Int. J. Greenh. Gas Control 5, 308–317.
Zhu, W.L., Li, M.B., Wu, P.K., 1997. The petroleum system in the Zhu III subbasin of the Pearl River Mouth basin. Petrol. Explor. Dev. 24, 21–23.
Zhu, W.L., Li, M.B., Wu, P.K., 1999. Petroleum systems of the zhu III subbasin, Pearl River mouth basin, South China sea. Am. Assoc. Pet. Geol. Bull. 83, 990–1003.
Zhu, W., Huang, B., Mi, L., Wilkins, R.W.T., Fu, N., Xiao, X., 2009. Geochemistry, origin, and deep–water exploration potential of natural gases in the Pearl River Mouth and Qiongdongnan basins, South China Sea. Am. Assoc. Pet. Geol. Bull. 93, 741–761.